Controls on the Occurrence of Submarine Landslides around Carbonate Platforms and Atolls in the Northwest South China Sea

Wei Li[1, 2]*†, Zhiyuan Cai[1, 2]†, Song Jing[1]*, Tiago M. Alves[3], Xiujuan Wang[4], Wenhuan Zhan[1, 2]

[1] *Laboratory of Ocean and Marginal Sea Geology, State Key Laboratory of Tropical Oceanography, South China Sea Institute of Oceanology, Chinese Academy of Sciences, Guangzhou 510301, China*

[2] *University of Chinese Academy of Sciences, Beijing 100049, China*

[3] *3D Seismic Lab, School of Earth and Environmental Sciences, Cardiff University, Main Building, Park Place, Cardiff, CF10 3AT, United Kingdom*

[4] *Submarine Geosciences and Prospecting Techniques, MOE and College of Marine Geosciences, Ocean University of China, Qingdao, 266100, China*

*Correspondence to: Dr. Wei Li (wli@scsio.ac.cn) and Dr. Song Jing (jingsong@scsio.ac.cn)

†These authors contributed equally to this work.

ABSTRACT

Submarine landslides are important hazards around carbonate platforms, posing a significant threat to coastal communities by generating tsunamis, while potentially damaging vital submarine infrastructure. Yet, the factors controlling slope instability near carbonate platforms remain poorly understood. In this study, we use high-resolution multibeam bathymetric and seismic reflection data to investigate submarine landslides on the flanks of carbonate platforms in the northwest South China Sea. We identify plastered and mounded contourite drifts that host submarine landslides of multiple sizes, with an area of 2.1 to 306 km² and failed volumes of 0.03 to 11.8 km³. A global comparison of failed contourite drifts reveals that slope angle around carbonate platforms is lower (~3.75°) than that on siliciclastic continental slopes (~8.93°). We attribute this difference to the lower shear strength of the predominantly calcareous contourite drifts around carbonate platforms and atolls compared with siliciclastic continental slopes. Our findings show that intrinsic sediment weakness is a critical control on slope instability around carbonate platforms, highlighting it as an underestimated geohazard in carbonate depositional environments. Our results provide crucial information to develop robust risk assessment strategies and safer engineering practices around carbonate platforms and atolls.

Keywords: Submarine landslide; Carbonate platform; Contourite drift; Slope instability; South China Sea

INTRODUCTION

Submarine landslides are geological features with an inherent potential to trigger large-scale seafloor deformation and associated tsunamis (Harbitz et al., 2014; Vanneste et al., 2014; Clare et al., 2023; Lenz et al., 2023). While being vastly documented on siliciclastic continental slopes, submarine landslides around carbonate platforms and atolls have thus far received comparatively limited attention in geohazard assessments. Yet, the proximity of inhabited islands to most carbonate platforms suggests that submarine landslides in such regions can pose a risk to coastal populations and to submarine infrastructure (Principaud et al., 2015; Tournadour et al., 2015; Mulder et al., 2019). On a global scale, mass-wasting events on the flanks of carbonate platforms, including those in northeast Australia (Puga-Bernabéu et al., 2017; Etienne et al., 2021), the Great Bahama Bank (Principaud et al., 2015; Tournadour et al., 2015; Le Goff et al., 2020), and the Xisha Uplift (Bai et al., 2022; Liu et al., 2023), also present a significant tsunamigenic risk. As an example, a 22 km^3 failure on the northern flank of the Puerto Rico carbonate platform, with an estimated sliding velocity of 40 m/s, may have led to a maximum tsunami runup height of 15.7 m in the past (Ten Brink et al., 2006).

The geological setting of carbonate platforms and atolls differs markedly from siliciclastic continental slopes. The development of carbonate platforms and atolls are governed by carbonate precipitation and the in-situ deposition of bioclastic material, which are both primarily driven by biological activity (Schlager et al., 1994; Wu et al., 2014; Wang et al., 2018). Hence, strata formed by the accumulation (and later consolidation) of bioclastic grains exhibit distinct geotechnical properties when compared to siliciclastic sediment, often recording a higher porosity and an inherently lower shear strength (Tanaka and Locat, 1999; Gaudin and White, 2009; Nugraha et al., 2022; Hussein et al., 2024). Furthermore, as evidenced by detailed outcrop studies, the mechanical behavior of such carbonate successions is strongly influenced by early diagenetic processes and syn-depositional deformation, which can fundamentally reorganise primary porosity and rock strength (Ogata et al., 2014a, 2014b; Lucca et al., 2024). In parallel, contourite drifts accumulated by bottom currents on many continental slopes, can also be present around carbonate platforms and atolls (Betzler and Eberli, 2019; Eberli and Betzler, 2019; Lüdmann et al., 2022; Bashah et al., 2024; Betzler et al., 2024). This is an important aspect as the presence of such drifts has been considered to control slope instability on siliciclastic continental slope (Weigelt and Uenzelmann-Neben, 2004; Miramontes et al., 2016; Miramontes et al., 2018; Liu et al., 2019; Li et al., 2024). Notwithstanding this fact, the factors preconditioning submarine landslides on contourite drifts accumulated around carbonate platforms remain poorly understood (Principaud et al., 2015; Lüdmann et al., 2022; Teixeira et al., 2024).

To investigate the difference in slope instability styles and inherent potential of contourite drifts deposited around carbonate platforms, we focus on the carbonate platforms and atolls dotting the Xisha Uplift of the South China Sea (SCS) (Fig. 1). High-resolution multibeam bathymetric and seismic data are used in this work to identify and characterize submarine landslides on the flanks of such carbonate platforms and atolls. We document the geotechnical properties and the Factors of Safety for contourite drifts accumulated on carbonate platforms to compare them with siliciclastic continental slopes that were drilled by the Ocean Drilling Program (ODP). By integrating regional and global data, this study aims to stress what are the factors preconditioning slope instability near carbonate platforms and atolls.

OCEANOGRAPHIC AND GEOLOGIC SETTINGS

Oceanographic Setting

Ocean currents have had a significant presence in the SCS throughout the Cenozoic (Su, 2004). During the Miocene, water-mass circulation was strongly influenced by exchanges with the Pacific Ocean through broad bathymetric lows (Qu et al., 2006; Tian et al., 2006; Yin et al., 2021; Wang et al., 2022). From the early Pliocene onward, the northward migration of the Luzon arc, and the subsequent (rapid) uplift of Taiwan, progressively restricted water-mass exchanges to establish the present-day, semi-enclosed circulation system of the SCS (Wang and Li, 2009). Present-day water-mass circulation involves a complex, multi-layered structure that is primarily driven by the inflow and outflow of water through the Luzon Strait (Fig. 1b). These water flows are closely influenced by regional monsoon patterns, with cyclonic (anticlockwise) surface waters being typically shallower than 300 m. Anticyclonic (clockwise) North Pacific Intermediate Water occurs at water depth between 300 and 1500 m, while the generally cyclonic deep waters occur below 1500 m (Su and Weng, 1994; Chen and Huang, 1996; Qu et al., 2006; Tian et al., 2006; Wang and Li, 2009; Cai et al., 2020).

The persistent ocean currents can generate multiple depositional and erosional features on nearby slopes. Relatively fast currents commonly form discrete mounded drifts adjacent to erosional moats, whereas slower currents favor the accumulation of plastered (sheeted) drifts that conform to the slope gradient (Faugères and Stow, 2008; Hernández-Molina et al., 2022) (Fig. 2). In the SCS, mounded and plastered drifts occur broadly on both the northern continental slope of the SCS and the flanks of carbonate platforms and atolls (Shao et al., 2007; Chen et al., 2016; Sun et al., 2017; Chen et al., 2022; Yu et al., 2022). The fine-grained nature and potentially lower shear strength of contourite deposits in the SCS have been related to multiple slope instability processes, from local submarine creep (Li et al., 2016; Gao et al., 2025) to large-scale submarine landslides (Li et al., 2014; Sun et al., 2018; Li et al., 2020).

Geologic Setting

The SCS has experienced an early syn-rifting stage before mid-Eocene (~45 Ma), a main syn-rifting stage until early-Miocene (~23 Ma), and a post-rifting stage to present (Fig. 3) (Dong et al., 2008; Ding et al., 2016; Cheng et al., 2021) (Fig. 3). Changes in tectonic subsidence and uplift following these tectonic stages, i.e., during the post-rift stage, resulted in further variations in sea-level throughout the northern SCS; in particular, a gradual sea level rise is recorded before Late Miocene (~11.6 Ma) and this was followed by a faster sea level rise afterward (Wu et al., 2014; Shao et al., 2017; Cheng et al., 2021).

Favored by the constant but progressive sea-level rise that accompanied continental breakup in the SCS, large carbonate platforms were first formed over the Xisha Uplift during the gradual sea level rise at the beginning of post-rifting stage (~23 Ma) (Ma et al., 2011; Wu et al., 2014; Qin et al., 2022). However, the acceleration in sea level rise recorded since Late Miocene (~11.6 Ma) (Shao et al., 2017), combined with a relative increase in siliciclastic input from the Indo-China Peninsula since the Pliocene (~5.5 Ma), have resulted in the progressive drowning and isolation of carbonate platforms on the Xisha Uplift (Wu et al., 2014; Qin et al., 2022). As a result, only those platforms in the central part of Xisha Uplift, where local structural highs are located, have remained emerged as atolls (Ma et al., 2011; Kuang et al., 2014; Wu et al., 2014) (Figs. 1b and 1c).

At least 11 drowned carbonate platforms and atolls are recognized on the Xisha Uplift at present (Fig. 1c). Drowned carbonate platforms include the Ganquan (GQCP), Zhongjianbei (ZJBCP), Zhongjian (ZJCP), and Zhaoshu (ZSCP) platforms. Evolving atolls, i.e., carbonate platforms not completely submerged, include the Beijiao (BJA), Huangguang (HGA), Langhua (LHA), Yuzhuo (YZA), Dongdao (DDA), Yongle (YLA), and Xuande (XDA) atolls (Ma et al., 2021; Bai et al., 2022) (Fig. 1c). Drowned carbonate platforms and still-emergent atolls are 10 km to 60 km apart, for an average distance of 36 km (Figs. 1b and 1c). The tops of drowned isolated carbonate platforms are relatively flat, occurring at water depths of 300 to 600 meters (Ma et al., 2021; Bai et al., 2022). In contrast, atolls contain local carbonate reefs that are exposed above sea level (Ma et al., 2011; Kuang et al., 2014; Wu et al., 2014) (Fig. 1c).

Seismic profiles acquired over the Xisha Uplift further reveal a distinct 'layer-cake' structure consisting of three main units: (1) a magmatic basement imaged as a chaotic, high-amplitude interval near the base of seismic profiles (Cheng et al., 2021); (2) drowned carbonate platforms and overlying atolls that grew on local basement highs and show continuous and parallel seismic reflections (Betzler et al., 2019; Qin et al., 2022; Chen et al., 2023); and (3) contourite drifts surrounding and draping the drowned carbonate platforms. These same drifts show sub-parallel and wavy reflections, onlapping the flanks of carbonate platforms (Fyhn et al., 2013; Betzler et al., 2019; Ma et al., 2021; Qin et al., 2022; Yu et al., 2022; Chen et al., 2023) (Fig. 4).

DATA AND METHODS

Seismic Reflection Data

Two-dimensional (2D) multi-channel seismic reflection data imaging the Xisha Uplift were acquired and processed by the China National Petroleum Corporation (CNPC). Assuming an average P-wave velocity of ~1500-2000 m/s in the shallow subsurface, the seismic data have a dominant frequency of approximately 30-60 Hz and yield an estimated vertical resolution of 6-16 m. The dataset has a trace spacing of 6.25 m and seismic interpretation was carried out using Kingdom® and Petrel® software packages. The vertical scales of the seismic profiles are presented in two-way travel time (TWT) in this work.

A sequence-stratigraphic framework was established for the study area by integrating seismic facies with lithological information and wireline data from exploration well LS22-1-1 (Fig. 3). The ages of seismic reflectors such as T20 (1.8 Ma), T30 (5.5 Ma), T40 (11.6 Ma), T50 (16 Ma), T60 (23 Ma), T70 (28.4 Ma) and Tg (45 Ma), were constrained by biostratigraphic data from well LS22-1-1 and then mapped in our seismic data (Sun et al., 2015; Cheng et al., 2021) (Figs. 3 and 4).

Geomorphic Data and Analysis

Multibeam bathymetric data covering the region around the Xisha Uplift were acquired using a hull-mounted SeaBeam 2112 multibeam echosounder system. Bathymetric data covers a water depth ranging from 34 m to 4471 m (Fig. 1b). The raw data were processed using CARIS HIPS® software, with the final bathymetric grid having a horizontal cell size of 100 m and a vertical resolution of 3 m (or 3‰ of the water depth). A processed digital elevation model (DEM) resulting from this bathymetric grid was imported into Global Mapper® software for visualization, geomorphic analyses, and mapping of submarine landslides and related features (e.g., contourite drifts and moats) (Fig. 5).

Several parameters were measured from the bathymetric data and seismic profiles to quantitatively characterize contourite drifts and their adjacent slopes. Slope Angle (α) was defined as the average gradient of the carbonate platforms' flanks or continental slope immediately adjacent to the contourite drift or landslide scar. It was measured perpendicularly to bathymetric contours (Figs. 2a and 2b). Mounded Drift Angle (β) is a property of detached, mounded drifts, where this angle is specifically measured on the steeper, landward-facing flank between the base of a drift (often a moat trough) and its crest (Fig. 2). Such a measurement is often considered in slope stability analyses. Plastered Drift Angle (γ) is measured on contourite drifts that are attached to a nearby slope and distributed along it. Measured either on bathymetric data or seismic reflection profiles, a moat trough is considered as the deepest point between a slope and the drift crest (Fig. 2b). Moat depth is further calculated by measuring the vertical distance from the moat trough to the drift crest (Fig. 2b). In parallel, moat width is measured as the horizontal distance from the crest of drift to the nearby slope (Fig. 2b).

In summary, geomorphic data from the Xisha Uplift were derived from the bathymetric and seismic data previously described. Comparative angle data for other carbonate platforms (e.g., Maldives, Bahamas, NE Australia) and continental slopes (e.g., NE SCS, NW Svalbard, NW Norwegian Sea, N Tyrrhenian Sea) were compiled from published seismic profiles and bathymetric data (see Supplementary Tables 01 and 02) and extracted from the PANGAEA data repository (Wilckens et al., 2023b).

Submarine Landslide Characterization

Submarine landslides can evacuate large volumes of sediments that are later emplaced as mass-transport deposits (MTDs). Distinct kinematic indicators can be preserved during the downslope movement of failed sediment, e.g., headwall and sidewall scarps as the upper and lateral boundary of a landslide scar, frontal ramps as the lower boundary of a landslide scar, and the glide plane between MTDs and underlying (intact) slope strata as basal detachment zones (Bull et al., 2009; Alves and Lourenço, 2010; Clare et al., 2018; Gamboa et al., 2021; Alves et al., 2022; Nugraha et al., 2022; Roger et al., 2024) (Figs. 6 and 7). The downslope transport of failed strata is accompanied by deformation, fragmentation and partial liquefaction, and, as a result, MTDs can exhibit chaotic to transparent and discontinuous seismic facies, in contrast to the parallel to sub-parallel, laterally continuous seismic facies that are characteristic of intact strata below and above (Sawyer et al., 2009; Camerlenghi et al., 2010; Etienne et al., 2021; Roger et al., 2024). Failed sediment can also contain blocky strata in which sub-parallel and continuous seismic reflectors are preserved inside, with chaotic seismic facies between blocks (Micallef et al., 2007; Alves, 2015; Alves et al., 2022).

In this work, the area of submarine landslides, the height of their headwall scarps and their local slope gradients are measured in 19 submarine landslides formed around the Xisha Uplift (see Table 1 for sources). The evacuated volume of failed material is estimated in this work using the model proposed by McAdoo et al. (2000) and *Equation 1*:

$$V = \frac{1}{2} A_s h cos\alpha$$

Equation 1

where A_s is the failed area, h is the headscarp height, α is slope angle taken from adjacent intact slope strata.

Morphometric parameters of other regions affected by submarine landslides, such as the Great Barrier Reef in northeast Australia, the west and east Atlantic continental margins, the Mediterranean Sea, the Antarctic and Arctic continental margins, are derived from Puga-Bernabéu et al. (2022) and Moscardelli and Wood (2015).

Calculation of a Factor of Safety (FOS)

To quantitatively assess and compare the static slope stability of contourite drifts, a Factor of Safety (FOS) was calculated assuming infinite slope conditions. An FOS value below 1.0 suggests that gravitational shear stress exceeds the shear strength of seafloor sediment, pointing out to potential slope instability under the conditions assumed in the calculations (Li et al., 2014; Steiner et al., 2015; Strupler et al., 2017; Miramontes et al., 2018). The FOS is thus calculated as the ratio of resisting shear strength to driving shear stress:

$$FOS = \frac{S_u(z)}{\sigma_v'(z) sin\alpha cos\alpha}$$

Equation 2

where S_u is the undrained shear strength of strata, σ_v' is the vertical effective stress, and α represents the slope angle.

Vertical effective stress (σ_v') is calculated via *Equation 3*:

$$\sigma_v' = \int_0^z \left(\left(\rho(z) - \rho_w(z)\right)g\right) dz$$

Equation 3

where ρ is the bulk density of sediments, ρ_w is the density of water, which is 1 g/cm^3, and g is gravitational acceleration (9.8 m/s^2).

Depth profiles for Bulk Density (ρ) and Undrained Shear Strength (S_u) - required for the above equations - were taken from publicly available data archives from the Ocean Drilling Program (ODP).

Data were compiled from nine (9) specific sites located on contourite drifts (Fig. 1a and Supplementary Table 03). Three of these locations are on contourite drifts around carbonate platforms (ODP Legs 133, 166 and 182), while six other locations are on contourite drifts accumulated on siliciclastic continental slopes (ODP Legs 105, 151, 157, 162, 178 and 188) (Fig. 1a).

RESULTS

Contourite Drifts on the Xisha Uplift

Within the Xisha Uplift, mounded and plastered drifts are widely distributed on the flanks of downed, isolated carbonate platforms and atolls. Plastered drifts are identified by their geometry - which follows the existing slope gradient - while mounded drifts are detached from nearby slopes by moats on upper slope (Fig. 2).

Plastered Drifts

In the Xisha Uplift, plastered drifts are mainly developed on the northwest flank of carbonate platforms and atolls, at a water depth between 600 and 1500 m, showing a wedge-shaped geometry that can be either convex or concave (Figs. 4b, 5a, 6a and 8b). Internally, they present onlapping, continuous, semi-transparent seismic reflections with a low to moderate amplitude and aggradational stacking patterns (Figs. 6d and 8c). Their thickness ranges from ~1000 ms TWT in the lower portion (at a water depth of 1500 m) to virtually zero in their shallow parts (Figs. 6a and 8b). Due to their close association with the carbonate platform/atoll flanks, the angle of these plastered drifts typically decreases to ~1° in their lower parts, reaching a maximum at their top where they inherit the underlying morphology of the carbonate platforms/atolls (Figs. 4 and 8b; see also Supplementary Table 01). The base of these drifts correlates with the T40 unconformity (~11.6 Ma, base Tortonian), which marks the cessation of carbonate platform growth due to the onset of fast sea level rise (Ma et al., 2011; Wu et al., 2014).

Mounded Drifts

Mounded drifts are mainly observed on the southeast flanks of carbonate platforms and atolls, such as the GQCP, XDA and ZJCP (Figs. 4b, 7, and 8e). Occurring at a water depth of 900 m to 1100 m, mounded drifts form convex depositional bodies with continuous, subparallel, and moderate-amplitude internal reflections (Figs. 4b, 7 and 8e). The average angle of these mounded drifts is ~ 4°, with the angle of nearby slopes approaching 13° (Supplementary Table 02). Mounded drift thickness varies from 300 ms TWT on the northeast flank of the XDA to c. 600 ms TWT on the southeast flank of the ZJCP (Figs. 7d and 8f). Plastered drifts are also identified at the base of the mounded drifts by the absence of a moat in their shallower portions (Fig. 8f). The base of these plastered drifts is also correlated with the T40 unconformity (~11.6 Ma, base Tortonian), indicating a Late Miocene age for their onset (Figs. 4b and 8f).

Erosional moats, representing areas of erosion or reduced deposition, show an average width of ~3.4 km and an average depth of 67 m (Supplementary Table 02). Erosional moats along the ZJCP reveal U-shaped and flat bases, which are up to 4.4 km wide and 157 m deep (Fig. 8f). Conversely, the moats that are closer to the XDA and the GQCP are V-shaped, 3 km to 4 km wide, and approximately 65 m deep (Figs. 4b and 7d).

Morphology of Contourite Drifts and Adjacent Slopes

A generally positive linear relationship is recorded between the slope angles of carbonate platforms/atolls and contourite drifts (Figs. 9a and 9b). The angle of mounded drifts ranges from 0° to 9°, with most being between 0° to 6° (Fig. 9a). In comparison, slope angle varies between 0° and 40°, with most values being between 0° to 15° (Figs. 9a). Plastered drifts show a more uniform geometry, with an angle ranging from 0° to 10°, while nearby platform and atoll slope angles vary from 0° to ~ 35° (Fig. 9b). Quantitative analyses show that the angles of the carbonate platform slopes are approximately three times greater than the angles of plastered drifts (Fig. 9b), and about six times greater than the angles of mounded drifts (Fig. 9a).

Submarine Landslides on the Xisha Uplift

Both recent and buried submarine landslides are observed on the Xisha Uplift. Recent landslides are identified by their distinct headwall and sidewall scarps and evacuated depressions on the seafloor, whereas buried landslides can be recognized as MTDs with their characteristic chaotic to transparent seismic facies.

Modern Submarine Landslides on Plastered Drifts

In this study, at least 18 modern submarine landslides are identified on plastered drifts formed adjacently to the GQCP, XDA, BJA, and HGA (Fig. 1c). Failed sediment ranges from 2.065 km^2 (Slide 13) to 306 km^2 (Slide 4), for an average area of 46 km^2 (Table 1). The volume of evacuated sediment estimated from Equation 1 varies from 0.028 km^3 (Slide 13) to 11.8 km^3 (Slide 4), for an average value of 1.2 km^3 (Table 1; Fig. 10). The three largest slides are located on the northwest flank of the XDA (Fig. 1c). Their headwall scarps are typically developed on the upper sections of plastered drifts at water depths of 600 to 800 m (Fig. 5). Submarine landslides, such as Slides 7 and 8 around the XDA, and Slides 11 and 12 around the BJA, were triggered at the middle of the plastered drifts (Figs. 5b and 5c). The angles of headwall and sidewall scarps vary from 5° for slides near the HGA, to 15° around the XDA, BJA, and GQCP (Fig. 5).

Modern Submarine Landslides on Mounded Drifts

While most observed landslides originate on plastered drifts, one particular submarine landslide (Slide 3) is recognized on the northeast flank of XDA over a mounded drift (Figs. 5b and 7). Compared to the landslides of plastered drifts, Slide 3 has a much longer headwall scarp (~20 km) and a smaller length/width ratio of 2.3, a value that contrast with an L/W ratio of 5.3 for typical plastered drift slides. In addition, Slide 3 has an area that approaches 70 km² and an estimated evacuated volume of 2.2 km³, making it significantly larger than most landslides identified on plastered drifts.

Buried MTDs in Contourite Drifts

Five distinct MTDs (MTDs 1-5) are identified in the interior of plastered drifts accumulated on the northwest flank of the GQCP (Figs. 6 and 8c). Occurring between Horizons T30 and T40 (Late Miocene), these MTDs reflect large-scale submarine instability near the GQCP. MTDs 1 and 2 have a similar thickness (~70 ms TWT) and appear to share a common basal glide plane (Figs. 6d and 8c). In contrast, MTD 3 is stratigraphically above MTDs 1 and 2, with its top reflection at Horizon T20, suggesting its occurrence at around 1.8 Ma (Fig. 6a).

MTDs 4 and 5 are found in the lower and upper parts of drift, respectively, within the Plio-Pleistocene strata that post-dates Horizon T20 (Figs. 6b and 6c). MTD 4 is c. 20 km long with a maximum thickness of 150 ms TWT (~120-150 m). Its headwall is not fully imaged in our seismic data, but its frontal ramp morphology, combined with chaotic seismic facies on its lower portion, are characteristic of frontally emerged MTDs (Fig. 6c). Slide blocks are observed in MTD 4 as relatively continuous strata in between chaotic intervals (Fig. 6c). MTD 5 is distinguished from MTD 4 by its chaotic and transparent seismic facies, reaching a maximum thickness of c. 50 ms TWT (~40-50 m) (Fig. 6b).

DISCUSSION

Relationship between Drifts Geometry and Slope Angle around Carbonate Platforms and Atolls

The morphology of drifts and associated erosional and depositional features are governed by the complex interplay between bottom current dynamics (velocity, interaction with topography), sediment supply and accommodation space (Wilckens et al., 2023a; 2023c). Our analysis confirms a positive correlation between the angles of contourite drifts and that of carbonate platforms and atoll flanks (Figs. 9a and 9b). However, when comparing our measurements with global data compilations, the relationship between contourite drifts and platform/atoll slope angles exhibits a less variability to siliciclastic continental slopes (Figs. 9a and 9b).

High sediment supply with low currents' energy may promote sediment aggradation, leading to a decrease in the number (and size) of erosional moats, the subsequent upslope migration of drift bodies, and relatively lower drift angles, as suggested by the contourite drifts imaged on the base of the slope near the GQCP and ZJCP (Figs. 4b and 8f). Such a relationship is also recorded in settings such as the Great Barrier Reef and Vietnam continental margin (Fyhn et al., 2013; Principaud et al., 2018; Betzler and Eberli, 2019). In contrast, low depositional rates, or stronger bottom currents, favor erosion to result in: a) more prominent moats, b) potentially steeper or more confined sediment drifts, as also documented in the Gulf of Cadiz (Hernández-Molina et al., 2008; Hernández-Molina et al., 2016; Wilckens et al., 2023a) and on the northeast flank of the XDA (Fig. 7b). The erosional moats and sediment drift on the northeast flank of XDA thus indicate the existence of intense bottom currents in the study area.

Our global compilation reveals that submarine landslides on plastered drifts around carbonate platforms and atolls typically fail at angles ranging from 0° to 10°, with the highest instability clustering at a dominant angle of c. 3.75° (Fig. 9c and Supplementary Table 4). In contrast, sediment failure on plastered drifts of siliciclastic continental slopes occurs at considerably steeper angles, usually between 5° and 15°, with a dominant angle of 8.93° (Fig. 9c). In parallel, while the volume of landslides on the Xisha Uplift is generally smaller than those occurred on siliciclastic continental slopes (Fig. 10), their broader distribution does not diminish their hazard potential. The slope failures in the study area represent significant mass-wasting events (up to 11.8 km^3 in volume), and their proximity to nearby islands and infrastructure (Figs. 5c and 5d) means that even moderate-sized failures may isolate these islands by severing underwater cables, potentially generating local tsunamis.

The combination of a lower failure angle threshold and the proximity to nearby, low-lying atolls highlights how underestimated these landslides are as geohazards.

Factors Controlling Slope Instability around Carbonate Platforms and Atolls

The greater potential instability of contourite drifts around the Xisha Uplift indicates other factors, in addition to inclination, that control slope instability at the same time. In this work, the strength of contourite drifts on both carbonate platforms/atolls and siliciclastic continental slopes were acquired from ODP databases and compared. While bulk densities of contourites are broadly similar between carbonate platforms/atolls (ODP legs 133, 166 and 182) and siliciclastic continental slopes (ODP legs 105, 151, 157, 162, 178 and 188), the undrained shear strength of carbonate sediment is consistently and significantly lower (Fig. 11b). This inherent weakness results in differing Factors of Safety (FOS), which are higher for drifts on siliciclastic continental slopes than around carbonate platforms and atolls (Fig. 11c).

The fundamental reason for this pronounced difference in shear strength should relate to specific lithology of the studied drifts (Brackenridge et al., 2018; Betzler and Eberli, 2019; Mulder et al., 2019; Bankole et al., 2020). Sediment drifts near carbonate platforms are predominantly composed of bioclastic and in-situ (precipitated) carbonate material derived from enhanced biological processes. In contrast, sediment drifts on siliciclastic continental slopes are typically dominated by siliciclastic material derived from terrestrial sources. For instance, in contourite drifts from the Blake-Bahama Outer Ridge, sediments transported from the Bahamas carbonate platforms contain more than 75% of carbonate bioclastic components, while those derived from the North American continental margin typically have less than 25% carbonate grains (Brandes, 2011). It is well-established that carbonate sediment, particularly fine-grained or poorly cemented sediment, has a lower shear strength, a higher initial porosity, a higher water content, greater compressibility, and potentially higher sensitivity, when compared to typical siliciclastic sediments (Tanaka and Locat, 1999; Gaudin and White, 2009; Brandes, 2011; Rashid et al., 2017; 2019; Gatter et al., 2021; Hussein et al., 2024).

Differences such as these can also be related to the distinct microstructure and composition of carbonate drifts. Clay and silt grains in siliciclastic deposits undergo mechanical compaction with burial, a character better expressed by their gradual decrease in porosity, and increase in shear strength, with depth (Bartetzko and Kopf, 2007, Hussein et al., 2024). Although the shear strength of carbonate sediment can also be influenced by both mechanic and diagenetic processes (Croize et al., 2010; Lebrec et al., 2024), the bioclastic particles in their interior limit early compaction via their internal clast-supported microstructure, resulting in a less pronounced increase in shear strength with depth and early compaction (Bartetzko and Kopf, 2007, Hussein et al., 2024). Our data suggest that even when considering diagenetic processes during burial, the inherent mechanical weakness of carbonate components in calcareous contourite drifts results in persistently low shear strength profiles (Fig. 11b). Therefore, the greater slope instability of sediment around carbonate platforms and atolls can be attributed to the mechanically weaker nature of their carbonate sediment (Figs. 11b and 12). This interpretation is further supported by a sensitivity analysis comparing the FOS of carbonate and siliciclastic plastered drifts across a realistic range of slope angles (Fig. S1). The analysis shows that, under identical contourite facies conditions, carbonate drifts are systematically less stable than their siliciclastic counterparts. This negative control demonstrates that the observed differences in slope stability are not a case-dependent artefact of a specific contourite facies, but are instead driven primarily by lithology. Although the FOS estimates rely on a simplified infinite-slope approach and the global compilation carries inherent comparability biases, the consistent relative offset between carbonate and siliciclastic drifts across angle ranges supports the robustness of the lithological interpretation.

High sedimentation rates contribute to slope instability by generating excess pore pressure and reducing effective stress in near-seafloor strata (Kvalstad et al., 2005; Laberg and Camerlenghi, 2008). However, long-term depositional rates for contourite drifts deposited near carbonate platforms and atolls are generally lower on the Xisha Uplift, Great Bahama Bank, and Maldives; such depositional rates vary from 2 to 13 cm/kyr (Betzler et al., 2016; Mulder et al., 2019; Qin et al., 2022; Betzler et al., 2024). On siliciclastic continental slopes such as those of the Norwegian and Tyrrhenian Seas, depositional rates vary from ~38 to 190 cm/kyr (Rasmussen et al., 1996; Mulder et al., 2003; Laberg and Vorren, 2004; Hernández-Molina et al., 2012; Martorelli et al., 2016). The excess pore pressure induced by rapid sediment loading can thus be excluded as a controlling factor for the enhanced instability of contourite drifts on carbonate platforms and atolls.

Styles of Contourite Drift Instability

The findings in this work reveal distinct slope instability styles that are dependent on drift type (mounded vs. plastered) and their inherent depositional settings (carbonate platform/atolls vs. siliciclastic continental slopes) (Fig. 12). Around carbonate platforms and atolls, there are two main instability styles: Type 1 involves failure originating from mounded drifts (Fig. 12a). Examples include submarine landslide S3 observed on the flank of the XDA (Fig. 7) and landslides documented in the Maldives (Lüdmann et al., 2022). Type 2 involves failures originating from plastered drifts (Fig. 12b). This appears to be the more prevalent failure style in carbonate depositional systems, representing most of the landslides documented around the Xisha Uplift (Fig. 5) and also on other major carbonate platforms and highs such as the Bahamas, Maldives, and Northeast Australia (Tournadour et al., 2015; Mulder et al., 2019; Lüdmann et al., 2022; Bashah et al., 2024).

On siliciclastic continental slopes, Type 3 reflects slope failure on large-scale mounded drifts (Fig. 12c). However, examples of major landslides that are specifically confined within large, mounded drifts on continental slopes seem relatively uncommon compared to a fourth type of slope instability, Type 4, which affects plastered drifts (Fig. 12d). Numerous examples of Type 4 are documented worldwide including the northeast continental margin of the SCS, sectors of the North Atlantic continental margin, and parts of the Mediterranean Sea (Miramontes et al., 2018; Miramontes et al., 2019; Osti et al., 2019; Gatter et al., 2020; Song et al., 2020; Chen et al., 2022; Wang et al., 2022).

Implications for Future Geohazard Assessments

This study highlights the significant, and perhaps previously underappreciated geohazard potential of submarine landslides originating from contourite drifts and atolls on the flanks of carbonate platforms. Relative to siliciclastic slopes bordering continental margins, drift-related landslides on carbonate platforms/atolls reveal a lower shear strength, a distinct lithology and stacking patterns. Our findings not only emphasize the importance of understanding sub-seafloor lithology in slope stability assessments, but also prove that relying solely on slope angle as a proxy of slope instability is a non-conservative approach in case contourite drifts are present.

The recognition of multiple submarine landslides on the Xisha Uplift, around the drowned carbonate platforms and still-emerged atolls, reveals how important it is to assess landslide risk around the latter. This is particularly the case when trying to assess potential landslide runout distances, and also their associated secondary hazards such as localized tsunamis.

CONCLUSIONS

Based on the analysis of multibeam bathymetry and seismic reflection data acquired around the Xisha Uplift, complemented by a comparative assessment of geotechnical properties from carbonate platforms, atolls, and siliciclastic continental slopes across the world, this work reveals that significantly gentler slope angles are sufficient to destabilize contourite drifts on carbonate platforms and atolls when compared to siliciclastic continental slopes. This research identifies the inherently weaker nature of carbonate sediment as the key factor controlling slope stability around carbonate platforms and atolls. The main conclusions of this work can thus be summarized as follows:

(1) Plastered and mounded contourite drifts developed around and over the Xisha Uplift constitute the primary location for submarine landslides.

(2) The influence of slope angle on the dip angle of contourite drifts appears less pronounced around carbonate platforms and atolls than on siliciclastic continental slopes.

(3) Contourite drifts surrounding carbonate platforms fail at significantly gentler slope angle (~3.75°) compared to their counterparts on siliciclastic continental slopes (with a predominant failure angle of ~8.93°).

(4) The predominantly carbonate nature of contourite drifts near carbonate platforms and atolls implies that sediment has a lower undrained shear strength compared to the typically stronger, siliciclastic-rich drifts found on siliciclastic continental slopes. This inherent weakness of carbonate slopes and drifts, primarily driven by lithology, is the critical factor controlling slope stability on these latter bathymetric features.

In summary, this study shows that understanding submarine geohazards on carbonate slopes implies a detailed acknowledgment of the critical role of low-strength carbonate-prone contourites, rather relying solely on slope angles. This is a critical insight for accurate geohazard assessments near oceanic islands, and for ensuring the safety of marine infrastructure and engineering work in these environments.

ACKNOWLEDGMENTS

We would like to acknowledge the China National Petroleum Corporation for the permissions to release the seismic data. Schlumberger (provider of Petrel®) is acknowledged for the provision of the academic licenses to State Key Laboratory of Tropical Oceanography, South China Sea Institute of Oceanology, Chinese Academy of Sciences, Guangzhou, China. Financial support for this research was provided by Hainan Provincial Natural Science Foundation of China (425CXTD623), National Natural Science Foundation of China (No. 42306070), Guangzhou Basic and Applied Basic Research Program (No. 2024A04J3812), Guangdong Basic and Applied Basic Research Foundation (2026A1515012197), and development fund of South China Sea Institute of Oceanology of the Chinese Academy of Sciences (SCSIO202206). The editors and two reviewers, including Kei Ogata and another anonymous reviewer, are thanked for their constructive comments that greatly help us improving the quality of our manuscript.

REFERENCE CITED

Alves, T.M., 2015, Submarine slide blocks and associated soft-sediment deformation in deep-water basins: A review: Marine and Petroleum Geology, v. 67, p. 262–285, doi:10.1016/j.marpetgeo.2015.05.010.

Alves, T.M., Cardona, S., and Rodrigues, M.C.N.L., 2022, Mass transport processes, injectites and styles of sediment remobilization, in Deepwater Sedimentary Systems, Elsevier, p. 361–406, doi:10.1016/B978-0-323-91918-0.00013-X.

Alves, T.M., and Lourenço, S.D.N., 2010, Geomorphologic features related to gravitational collapse: Submarine landsliding to lateral spreading on a Late Miocene–Quaternary slope (SE Crete, eastern Mediterranean): Geomorphology, v. 123, p. 13–33, doi:10.1016/j.geomorph.2010.04.030.

Bai, H., Sun, Y., Wang, D., Wang, W., and Wu, S., 2022, Geophysical Evidence for Carbonate Platform Periphery Gravity Flows in the Xisha Islands, South China Sea: Journal of Ocean University of China, v. 21, p. 837–848, doi:10.1007/s11802-022-5099-7.

Bankole, S., Buckman, J., and Stow, D., 2020, Unusual Components Within a Fine-Grained Contourite Deposit: Significance for Interpretation of Provenance and the Contourite Budget: Minerals, v. 10, p. 488, doi:10.3390/min10060488.

Bartetzko, A., and Kopf, A. J. (2007). The relationship of undrained shear strength and porosity with depth in shallow (<50 m) marine sediments. Sedimentary Geology, 196, 235–249, doi:10.1016/j.sedgeo.2006.04.005

Bashah, S., Eberli, G.P., and Anselmetti, F.S., 2024, Archive for the East Australian Current: carbonate contourite depositional system on the Marion Plateau, Northeast Australia: Marine Geology, v. 469, p. 107224, doi:10.1016/j.margeo.2024.107224.

Betzler, C. et al., 2024, Dismantling of an isolated tropical carbonate platform through flank collapse and canyon erosion, Coral Sea, Northeast Australia: Marine Geology, v. 475, p. 107361, doi:10.1016/j.margeo.2024.107361.

Betzler, C.G. et al., 2016, International Ocean Discovery Program Expedition 359 preliminary report: Maldives monsoon and sea level:, doi:10.14379/iodp.pr.359.2016.

Betzler, C., and Eberli, G.P., 2019, Miocene start of modern carbonate platforms: Geology, v. 47, p. 771–775, doi:10.1130/G45994.1.

Brackenridge, R.E. et al., 2018, Textural characteristics and facies of sand ‐ rich contourite depositional systems (M. Marzo, Ed.): Sedimentology, v. 65, p. 2223–2252, doi:10.1111/sed.12463.

Brandes, H.G., 2011, Geotechnical characteristics of deep-sea sediments from the North Atlantic and North Pacific oceans: Ocean Engineering, v. 38, p. 835–848, doi:10.1016/j.oceaneng.2010.09.001.

Bull, S., Cartwright, J., and Huuse, M., 2009, A review of kinematic indicators from mass-transport complexes using 3D seismic data: Marine and Petroleum Geology, v. 26, p. 1132–1151, doi:10.1016/j.marpetgeo.2008.09.011.

Cai, Z., Gan, J., Liu, Z., Hui, C.R., and Li, J., 2020, Progress on the formation dynamics of the layered circulation in the South China Sea: Progress in Oceanography, v. 181, p. 102246, doi:10.1016/j.pocean.2019.102246.

Camerlenghi, A., Urgeles, R., and Fantoni, L., 2010, A Database on Submarine Landslides of the Mediterranean Sea, in Submarine Mass Movements and Their Consequences, Dordrecht, Springer Netherlands, p. 503–513, doi:10.1007/978-90-481-3071-9_41.

Chen, C.-T.A., and Huang, M.-H., 1996, A mid-depth front separating the South China Sea water and the Philippine sea water: Journal of Oceanography, v. 52, p. 17–25, doi:10.1007/BF02236530.

Chen, W., Wu, S., Wang, D., Betzler, C., and Ma, Y., 2023, Stratigraphic evolution and drowning steps of a submerged isolated carbonate platform in the northern South China Sea: Frontiers in Marine Science, v. 10, p. 1200788, doi:10.3389/fmars.2023.1200788.

Chen, H., Xie, X., Zhang, W., Shu, Y., Wang, D., Vandorpe, T., and Van Rooij, D., 2016, Deep-water sedimentary systems and their relationship with bottom currents at the intersection of Xisha Trough and Northwest Sub-Basin, South China Sea: Marine Geology, v. 378, p. 101–113, doi:10.1016/j.margeo.2015.11.002.

Chen, H., Zhang, W., Xie, X., Gao, Y., Liu, S., Ren, J., Wang, D., and Su, M., 2022, Linking oceanographic processes to contourite features: Numerical modelling of currents influencing a contourite depositional system on the northern South China Sea margin: Marine Geology, v. 444, p. 106714, doi:10.1016/j.margeo.2021.106714.

Cheng, C., Jiang, T., Kuang, Z., Ren, J., Liang, J., Lai, H., and Xiong, P., 2021, Seismic characteristics and distributions of Quaternary mass transport deposits in the Qiongdongnan Basin, northern South China Sea: Marine and Petroleum Geology, v. 129, p. 105118, doi:10.1016/j.marpetgeo.2021.105118.

Clare, M. et al., 2018, A consistent global approach for the morphometric characterization of subaqueous landslides: 8th International Symposium on Submarine Mass Movements and Their Consequences, ISSMMTC 2018, p. 455–477, doi:10.1144/SP477.15.

Clare, M.A. et al., 2023, Fast and destructive density currents created by ocean-entering volcanic eruptions: Science, v. 381, p. 1085–1092, doi:10.1126/science.adi3038.

Croize, D., Bjørlykke, K., Jahren, J., and Renard, F., 2010, Experimental mechanical and chemical compaction of carbonate sand: Journal of Geophysical Research: Solid Earth, v. 115, p. 1–17, doi:10.1029/2010JB007697.

Ding, W., Li, J., and Clift, P.D., 2016, Spreading dynamics and sedimentary process of the Southwest Sub-basin, South China Sea: Constraints from multi-channel seismic data and IODP Expedition 349: Journal of Asian Earth Sciences, v. 115, p. 97–113, doi:10.1016/j.jseaes.2015.09.013.

Dong, D., Wu, S., Zhang, G., and Yuan, S., 2008, Rifting process and formation mechanisms of syn-rift stage prolongation in the deepwater basin, northern South China Sea: Chinese Science Bulletin, v. 53, p. 3715–3725, doi:10.1007/s11434-008-0326-1.

Eberli, G.P., and Betzler, C., 2019, Characteristics of modern carbonate contourite drifts (T. Frank, Ed.): Sedimentology, v. 66, p. 1163–1191, doi:10.1111/sed.12584.

Etienne, S. et al., 2021, Large-scale margin collapses along a partly drowned, isolated carbonate platform (Lansdowne Bank, SW Pacific Ocean): Marine Geology, v. 436, p. 106477, doi:10.1016/j.margeo.2021.106477.

Faugères, J.-C., and Stow, D.A.V., 2008, Chapter 14 Contourite Drifts, in Developments in Sedimentology, v. 60, p. 257–288, doi:10.1016/S0070-4571(08)10014-0.

Fyhn, M.B.W., Boldreel, L.O., Nielsen, L.H., Giang, T.C., Nga, L.H., Hong, N.T.M., Nguyen, N.D., and Abatzis, I., 2013, Carbonate platform growth and demise offshore Central Vietnam: Effects of Early Miocene transgression and subsequent onshore uplift: Journal of Asian Earth Sciences, v. 76, p. 152–168, doi:10.1016/j.jseaes.2013.02.023.

Gamboa, D., Omira, R., and Terrinha, P., 2021, A database of submarine landslides offshore West and Southwest Iberia: Scientific Data, v. 8, p. 1–9, doi:10.1038/s41597-021-00969-w.

Gao, W., Li, W., Alves, T.M., Jing, S., and Zhan, W., 2025, Why does widespread submarine creep occur on the low-gradient continental slope of the northern South China Sea? Marine and Petroleum Geology, v. 180, p. 107453, doi:10.1016/j.marpetgeo.2025.107453.

Gatter, R., Clare, M.A., Hunt, J.E., Watts, M., Madhusudhan, B.N., Talling, P.J., and Huhn, K., 2020, A multi-disciplinary investigation of the AFEN Slide: the relationship between contourites and submarine landslides: Geological Society, London, Special Publications, v. 500, p. 173–193, doi:10.1144/SP500-2019-184.

Gatter, R., Clare, M.A., Kuhlmann, J., and Huhn, K., 2021, Characterisation of weak layers, physical controls on their global distribution and their role in submarine landslide formation: Earth-Science Reviews, v. 223, p. 103845, doi:10.1016/j.earscirev.2021.103845.

Gaudin C. and White D.J., 2009, New centrifuge modelling techniques for investigating seabed pipeline behaviour, in Proceedings of the 17th International Conference on Soil Mechanics and Geotechnical Engineering, IOS Press, doi:10.3233/978-1-60750-031-5-448.

Harbitz, C.B., Løvholt, F., and Bungum, H., 2014, Submarine landslide tsunamis: how extreme and how likely? Natural Hazards, v. 72, p. 1341–1374, doi:10.1007/s11069-013-0681-3.

Hernández-Molina, F.J. et al., 2012, Integrated Ocean Drilling Program Expedition 339 Preliminary Report: Mediterranean Outflow: Environmental significance of the Mediterranean Outflow water and its global implications: 16 November 2011-16 January 2012:, doi:10.2204/iodp.pr.339.2012.

Hernández-Molina, F.J. et al., 2016, Oceanographic processes and morphosedimentary products along the Iberian margins: A new multidisciplinary approach: Marine Geology, v. 378, p. 127–156, doi:10.1016/j.margeo.2015.12.008.

Hernández-Molina, F.J. et al., 2022, Contourites and mixed depositional systems: A paradigm for deepwater sedimentary environments: 301–360 p., doi:10.1016/B978-0-323-91918-0.00004-9.

Hernández-Molina, F.J., Llave, E., and Stow, D.A.V., 2008, Chapter 19 Continental Slope Contourites, in Developments in Sedimentology, Elsevier, v. 60, p. 379–408, doi:10.1016/S0070-4571(08)10019-X.

Hussein, A.A.A., Zhao, L., Al-Masgari, A.A.-S.A., and Handoyo, H., 2024, Shear strength characteristics of marine sediments: the influences of lithofacies and sedimentological environment: Marine Geophysical Research, v. 45, p. 14, doi:10.1007/s11001-024-09545-4.

Kuang, Z., Guo, Y., Wang, L., Liang, J., and Sha, Z., 2014, Evolution of the Late Miocene atoll systems offshore Xisha Islands: Science China Earth Sciences, v. 57, p. 3084–3096, doi:10.1007/s11430-014-4962-9.

Kvalstad, T.J., Andresen, L., Forsberg, C.F., Berg, K., Bryn, P., and Wangen, M., 2005, The Storegga slide: evaluation of triggering sources and slide mechanics: Marine and Petroleum Geology, v. 22, p. 245–256, doi:10.1016/j.marpetgeo.2004.10.019.

Laberg, J.S., and Camerlenghi, A., 2008, Chapter 25 The Significance of Contourites for Submarine Slope Stability, in Developments in Sedimentology, Elsevier, v. 60, p. 537–556, doi:10.1016/S0070-4571(08)10025-5.

Laberg, J.S., and Vorren, T.O., 2004, Weichselian and Holocene growth of the northern high-latitude Lofoten Contourite Drift on the continental slope of Norway: Sedimentary Geology, v. 164, p. 1–17, doi:10.1016/j.sedgeo.2003.07.004.

Lebrec, U., Sharma, S., Watson, P., Riera, R., Joer, H., Beemer, R., and Gaudin, C., 2024, A study of the effects of early diagenesis on the geotechnical properties of carbonate sediments (North West Shelf, Australia): Scientific Reports, v. 14, p. 1–19, doi:10.1038/s41598-024-67207-2.

Le Goff, J., Slootman, A., Mulder, T., Cavailhes, T., Ducassou, E., Hanquiez, V., Jaballah, J., and Reijmer, J.J.G., 2020, On the architecture of intra-formational Mass-Transport Deposits: Insights from the carbonate slopes of Great Bahama Bank and the Apulian Carbonate Platform: Marine Geology, v. 427, p. 106205, doi:10.1016/j.margeo.2020.106205.

Lenz, B.L., Griffith, W.A., and Sawyer, D.E., 2023, Impact‐Induced Seafloor Deformation From Submarine Landslides: Diagnostic of Slide Velocity? Geophysical Research Letters, v. 50, p. e2023GL104818, doi:10.1029/2023GL104818.

Li, W., Alves, T.M., Rebesco, M., Sun, J., Li, J., Li, S., and Wu, S., 2020, The Baiyun Slide Complex, South China Sea: A modern example of slope instability controlling submarine-channel incision on continental slopes: Marine and Petroleum Geology, v. 114, p. 104231, doi:10.1016/j.marpetgeo.2020.104231.

Li, W., Alves, T.M., Wu, S., Rebesco, M., Zhao, F., Mi, L., and Ma, B., 2016, A giant, submarine creep zone as a precursor of large-scale slope instability offshore the Dongsha Islands (South China Sea): Earth and Planetary Science Letters, v. 451, p. 272–284, doi:10.1016/j.epsl.2016.07.007.

Li, W., Krastel, S., Alves, T.M., Jing, S., Rebesco, M., Gross, F., Urlaub, M., and Georgiopoulou, A., 2024, Origin, evolution and significance of giant buried sediment mounds near the Sahara Slide Complex, North‐west African margin: Sedimentology, v. 71, p. 1436–1456, doi:10.1111/sed.13182.

Li, W., Wu, S., Völker, D., Zhao, F., Mi, L., and Kopf, A., 2014, Morphology, seismic characterization and sediment dynamics of the Baiyun Slide Complex on the northern South China Sea margin: Journal of the Geological Society, v. 171, p. 865–877, doi:10.1144/jgs2014-034.

Liu, S., Van Rooij, D., Vandorpe, T., González-Pola, C., Ercilla, G., and Hernández-Molina, F.J., 2019, Morphological features and associated bottom-current dynamics in the Le Danois Bank region (southern Bay of Biscay, NE Atlantic): A model in a topographically constrained small basin: Deep Sea Research Part I: Oceanographic Research Papers, v. 149, p. 103054, doi:10.1016/j.dsr.2019.05.014.

Liu, G., Wang, D., Chen, W., Wang, W., Betzler, C., and Han, X., 2023, Submarine landslides on a carbonate platform slope changing transport pathways of deepwater gravity flows: Insights from the Xisha Islands, South China Sea: Geomorphology, v. 437, p. 108813, doi:10.1016/j.geomorph.2023.108813.

Lüdmann, T., Betzler, C., Lindhorst, S., Lahajnar, N., and Hübscher, C., 2022, Submarine landsliding in carbonate ooze along low-angle slopes (Inner Sea, Maldives): Marine and Petroleum Geology, v. 136, p. 105403, doi:10.1016/j.marpetgeo.2021.105403.

Lucca, A., Ogata, K., Balsamo, F., Borsani, A., Clemenzi, L., Hatushika, R., Tinterri, R., and Storti, F., 2024, Sedimentary facies control on fracture and mechanical stratigraphy in siliciclastics: Marnoso-arenacea formation, Northern Apennines, Italy: Marine and Petroleum Geology, v. 167, p. 106927, doi:10.1016/j.marpetgeo.2024.106927.

Ma, B., Qin, Z., Wu, S., Cai, G., Li, X., Wang, B., Liu, X., Qin, Y., and Huang, X., 2021, High-resolution acoustic data revealing periplatform sedimentary characteristics in the Xisha Archipelago, South China Sea: Interpretation, v. 9, p. T533–T547, doi:10.1190/INT-2020-0093.1.

Ma, Y., Wu, S., Lv, F., Dong, D., Sun, Q., Lu, Y., and Gu, M., 2011, Seismic characteristics and development of the Xisha carbonate platforms, northern margin of the South China Sea: Journal of Asian Earth Sciences, v. 40, p. 770–783, doi:10.1016/j.jseaes.2010.11.003.

Martorelli, E., Bosman, A., Casalbore, D., and Falcini, F., 2016, Interaction of down-slope and along-slope processes off Capo Vaticano (southern Tyrrhenian Sea, Italy), with particular reference to contourite-related landslides: Marine Geology, v. 378, p. 43–55, doi:10.1016/j.margeo.2016.01.005.

McAdoo, B.G., Pratson, L.F., and Orange, D.L., 2000, Submarine landslide geomorphology, US continental slope: Marine Geology, v. 169, p. 103–136, doi:10.1016/S0025-3227(00)00050-5.

Micallef, A., Masson, D.G., Berndt, C., and Stow, D.A.V., 2007, Morphology and mechanics of submarine spreading: A case study from the Storegga Slide: Journal of Geophysical Research: Earth Surface, v. 112, p. 1–21, doi:10.1029/2006JF000739.

Miller, K.G., Browning, J.V., Schmelz, W.J., Kopp, R.E., Mountain, G.S., and Wright, J.D., 2020, Cenozoic sea-level and cryospheric evolution from deep-sea geochemical and continental margin records: Science Advances, v. 6, doi:10.1126/sciadv.aaz1346.

Miramontes, E., Cattaneo, A., Jouet, G., Théreau, E., Thomas, Y., Rovere, M., Cauquil, E., and Trincardi, F., 2016, The Pianosa Contourite Depositional System (Northern Tyrrhenian Sea): Drift morphology and Plio-Quaternary stratigraphic evolution: Marine Geology, v. 378, p. 20–42, doi:10.1016/j.margeo.2015.11.004.

Miramontes, E., Garreau, P., Caillaud, M., Jouet, G., Pellen, R., Hernández-Molina, F.J., Clare, M.A., and Cattaneo, A., 2019, Contourite distribution and bottom currents in the NW Mediterranean Sea: Coupling seafloor geomorphology and hydrodynamic modelling: Geomorphology, v. 333, p. 43–60, doi:10.1016/j.geomorph.2019.02.030.

Miramontes, E., Garziglia, S., Sultan, N., Jouet, G., and Cattaneo, A., 2018, Morphological control of slope instability in contourites: a geotechnical approach: Landslides, v. 15, p. 1085–1095, doi:10.1007/s10346-018-0956-6.

Moscardelli, L., and Wood, L., 2015, Morphometry of mass-transport deposits as a predictive tool: Geological Society of America Bulletin, p. B31221.1, doi:10.1130/B31221.1.

Mulder, T. et al., 2019, Contour current imprints and contourite drifts in the Bahamian archipelago (C. Betzler, Ed.): Sedimentology, v. 66, p. 1192–1221, doi:10.1111/sed.12587.

Mulder, T. et al., 2003, The Gulf of Cadiz: an unstable giant contouritic levee: Geo-Marine Letters, v. 23, p. 7–18, doi:10.1007/s00367-003-0119-0.

Nugraha, H.D., Jackson, C.A.-L., Johnson, H.D., Hodgson, D.M., and Clare, M.A., 2022, Extreme erosion by submarine slides: Geology, v. 50, p. 1130–1134, doi:10.1130/G50164.1.

Ogata, K., Pogačnik, Ž., Pini, G.A., Tunis, G., Festa, A., Camerlenghi, A., and Rebesco, M., 2014a, The carbonate mass transport deposits of the Paleogene Friuli Basin (Italy/Slovenia): Internal anatomy and inferred genetic processes: Marine Geology, v. 356, p. 88–110, doi:10.1016/j.margeo.2014.06.014.

Ogata, K., Senger, K., Braathen, A., and Tveranger, J., 2014b, Fracture corridors as seal-bypass systems in siliciclastic reservoir-cap rock successions: Field-based insights from the Jurassic Entrada Formation (SE Utah, USA): Journal of Structural Geology, v. 66, p. 162–187, doi:10.1016/j.jsg.2014.05.005.

Osti, G., Waghorn, K.A., Waage, M., Plaza-Faverola, A., and Ferré, B., 2019, Evolution of contourite drifts in regions of slope failures at eastern Fram Strait: arktos, v. 5, p. 105–120, doi:10.1007/s41063-019-00070-y.

Principaud, M., Mulder, T., Gillet, H., and Borgomano, J., 2015, Large-scale carbonate submarine mass-wasting along the northwestern slope of the Great Bahama Bank (Bahamas): Morphology, architecture, and mechanisms: Sedimentary Geology, v. 317, p. 27–42, doi:10.1016/j.sedgeo.2014.10.008.

Principaud, M., Mulder, T., Hanquiez, V., Ducassou, E., Eberli, G.P., Chabaud, L., and Borgomano, J., 2018, Recent morphology and sedimentary processes along the western slope of Great Bahama Bank (Bahamas) (J. Reijmer, Ed.): Sedimentology, v. 65, p. 2088–2116, doi:10.1111/sed.12458.

Puga-Bernabéu, Á., Beaman, R.J., Webster, J.M., Thomas, A.L., and Jacobsen, G., 2017, Gloria Knolls Slide: A prominent submarine landslide complex on the Great Barrier Reef margin of north-eastern Australia: Marine Geology, v. 385, p. 68–83, doi:10.1016/j.margeo.2016.12.008.

Puga-Bernabéu, Á., López-Cabrera, J., Webster, J.M., and Beaman, R.J., 2022, Submarine landslide morphometrics and slope failure dynamics along a mixed carbonate-siliciclastic margin, north-eastern Australia: Geomorphology, v. 403, p. 108179, doi:10.1016/j.geomorph.2022.108179.

Qin, Y., Wu, S., and Betzler, C., 2022, Backstepping patterns of an isolated carbonate platform in the northern South China Sea and its implication for paleoceanography and paleoclimate: Marine and Petroleum Geology, v. 146, p. 105927, doi:10.1016/j.marpetgeo.2022.105927.

Qu, T., Girton, J.B., and Whitehead, J.A., 2006, Deepwater overflow through Luzon Strait: Journal of Geophysical Research: Oceans, v. 111, p. 2005JC003139, doi:10.1029/2005JC003139.

Rashid, H., MacKillop, K., Sherwin, J., Piper, D.J.W., Marche, B., and Vermooten, M., 2017, Slope instability on a shallow contourite-dominated continental margin, southeastern Grand Banks, eastern Canada: Marine Geology, v. 393, p. 203–215, doi:10.1016/j.margeo.2017.01.001.

Rashid, H., Piper, D.J.W., MacKillop, K., Ouellette, D., Vermooten, M., Muñoz, A., and Jiménez, P., 2019, Dynamics of sediments on a glacially influenced, sediment starved, current-swept continental margin: The SE Grand Banks Slope off Newfoundland: Marine Geology, v. 408, p. 67–86, doi:10.1016/j.margeo.2018.11.012.

Rasmussen, T.L., Van Weering, Tj.C.E., and Labeyrie, L., 1996, High resolution stratigraphy of the Faeroe-Shetland Channel and its relation to North Atlantic paleoceanography: the last 87 kyr: Marine Geology, v. 131, p. 75–88, doi:10.1016/0025-3227(95)00145-X.

Rebesco, M., Hernández-Molina, F.J., Van Rooij, D., and Wåhlin, A., 2014, Contourites and associated sediments controlled by deep-water circulation processes: State-of-the-art and future considerations: Marine Geology, v. 352, p. 111–154, doi:10.1016/j.margeo.2014.03.011.

Roger, J.H.M. et al., 2024, A review of approaches for submarine landslide-tsunami hazard identification and assessment: Marine and Petroleum Geology, v. 162, p. 106729, doi:10.1016/j.marpetgeo.2024.106729.

Sawyer, D.E., Flemings, P.B., Dugan, B., and Germaine, J.T., 2009, Retrogressive failures recorded in mass transport deposits in the Ursa Basin, Northern Gulf of Mexico: Journal of Geophysical Research: Solid Earth, v. 114, p. 1–20, doi:10.1029/2008JB006159.

Schlager, W., Reijmer, J.J.G., and Droxler, A., 1994, Highstand Shedding of Carbonate Platforms: SEPM Journal of Sedimentary Research, v. Vol. 64B, p. 270–281, doi:10.1306/D4267FAA-2B26-11D7-8648000102C1865D.

Shao, L., Cui, Y., Qiao, P., Zhang, D., Liu, X., and Zhang, C., 2017, Sea-level changes and carbonate platform evolution of the Xisha Islands (South China Sea) since the Early Miocene: Palaeogeography, Palaeoclimatology, Palaeoecology, v. 485, p. 504–516, doi:10.1016/j.palaeo.2017.07.006.

Shao, L., Li, X., Geng, J., Pang, X., Lei, Y., Qiao, P., Wang, L., and Wang, H., 2007, Deep water bottom current deposition in the northern South China Sea: Science in China Series D: Earth Sciences, v. 50, p. 1060–1066, doi:10.1007/s11430-007-0015-y.

Song, J., Alves, T.M., Omosanya, K.O., Hales, T.C., and Ze, T., 2020, Tectonic evolution of strike-slip zones on continental margins and their impact on the development of submarine landslides (Storegga Slide, northeast Atlantic): GSA Bulletin, v. 132, p. 2397–2414, doi:10.1130/B35421.1.

Steiner, A., Kopf, A.J., Henry, P., Stegmann, S., Apprioual, R., and Pelleau, P., 2015, Cone penetration testing to assess slope stability in the 1979 Nice landslide area (Ligurian Margin, SE France): Marine Geology, v. 369, p. 162–181, doi:10.1016/j.margeo.2015.08.008.

Strupler, M., Hilbe, M., Anselmetti, F.S., Kopf, A.J., Fleischmann, T., and Strasser, M., 2017, Probabilistic stability evaluation and seismic triggering scenarios of submerged slopes in Lake Zurich (Switzerland): Geo-Marine Letters, v. 37, p. 241–258, doi:10.1007/s00367-017-0492-8.

Su, J., 2004, Overview of the South China Sea circulation and its influence on the coastal physical oceanography outside the Pearl River Estuary: Continental Shelf Research, v. 24, p. 1745–1760, doi:10.1016/j.csr.2004.06.005.

Su, M., Xie, X., Xie, Y., Wang, Z., Zhang, C., Jiang, T., and He, Y., 2014, The segmentations and the significances of the Central Canyon System in the Qiongdongnan Basin, northern South China Sea: Journal of Asian Earth Sciences, v. 79, p. 552–563, doi:10.1016/j.jseaes.2012.12.038.

Su, Y., and Weng, X., 1994, Water Masses in China Seas, in Di, Z., Yuan-Bo, L., and Cheng-Kui, Z. eds., Oceanology of China Seas, Dordrecht, Springer Netherlands, p. 3–16, doi:10.1007/978-94-011-0862-1_2.

Sun, Q., Cartwright, J., Lüdmann, T., Wu, S., and Yao, G., 2017, Three-dimensional seismic characterization of a complex sediment drift in the South China Sea: Evidence for unsteady flow regime (J. Trofimovs, Ed.): Sedimentology, v. 64, p. 832–853, doi:10.1111/sed.12330.

Sun, Q., Cartwright, J., Xie, X., Lu, X., Yuan, S., and Chen, C., 2018, Reconstruction of repeated Quaternary slope failures in the northern South China Sea: Marine Geology, v. 401, p. 17–35, doi:10.1016/j.margeo.2018.04.009.

Sun, Z., Wang, Z., Sun, Z., Wang, Z., Zhang, W., and He, L., 2015, Structure and kinematic analysis of the deepwater area of the Qiongdongnan Basin through a seismic interpretation and analogue modeling experiments: Acta Oceanologica Sinica, v. 34, p. 32–40, doi:10.1007/s13131-015-0585-z.

Tanaka, H., and Locat, J., 1999, A microstructural investigation of Osaka Bay clay: the impact of microfossils on its mechanical behaviour: Canadian Geotechnical Journal, v. 36, p. 493–508, doi:10.1139/t99-009.

Teixeira, M., Roque, C., Omira, R., Marques, F., Gamboa, D., Terrinha, P., Ercilla, G., Yenes, M., Mena, A., and Casas, D., 2024, Submarine landslide hazard in the Sines Contourite Drift, SW Iberia: slope instability analysis under static and transient conditions: Natural Hazards, v. 120, p. 3505–3531, doi:10.1007/s11069-023-06340-z.

Ten Brink, U.S., Geist, E.L., and Andrews, B.D., 2006, Size distribution of submarine landslides and its implication to tsunami hazard in Puerto Rico: Geophysical Research Letters, v. 33, p. 2006GL026125, doi:10.1029/2006GL026125.

Tian, J., Yang, Q., Liang, X., Xie, L., Hu, D., Wang, F., and Qu, T., 2006, Observation of Luzon Strait transport: Geophysical Research Letters, v. 33, p. 2006GL026272, doi:10.1029/2006GL026272.

Tournadour, E., Mulder, T., Borgomano, J., Hanquiez, V., Ducassou, E., and Gillet, H., 2015, Origin and architecture of a Mass Transport Complex on the northwest slope of Little Bahama Bank (Bahamas): Relations between off-bank transport, bottom current sedimentation and submarine landslides: Sedimentary Geology, v. 317, p. 9–26, doi:10.1016/j.sedgeo.2014.10.003.

Vanneste, M., Sultan, N., Garziglia, S., Forsberg, C.F., and L'Heureux, J.-S., 2014, Seafloor instabilities and sediment deformation processes: The need for integrated, multi-disciplinary investigations: Marine Geology, v. 352, p. 183–214, doi:10.1016/j.margeo.2014.01.005.

Wang, X., Cai, F., Sun, Z., Li, Q., Li, A., Sun, Y., Zhong, W., and Sun, Q., 2022, Late Miocene–Quaternary seismic stratigraphic responses to tectonic and climatic changes at the northeastern margin of the South China Sea: GSA Bulletin, v. 134, p. 2611–2632, doi:10.1130/B36224.1.

Wang, P., and Li, Q. (Eds.), 2009, The South China Sea: Dordrecht, Springer Netherlands, Developments in Paleoenvironmental Research, v. 13, doi:10.1007/978-1-4020-9745-4.

Wang, W., Wang, D., Wu, S., Völker, D., Zeng, H., Cai, G., and Li, Q., 2018, Submarine landslides on the north continental slope of the South China Sea: Journal of Ocean University of China, v. 17, p. 83–100, doi:10.1007/s11802-018-3491-0.

Weigelt, E., and Uenzelmann-Neben, G., 2004, Sediment deposits in the Cape Basin: Indications for shifting ocean currents? AAPG Bulletin, v. 88, p. 765–780, doi:10.1306/01260403101.

Wilckens, H. et al., 2023a, Factors controlling the morphology and internal sediment architecture of moats and their associated contourite drifts: Sedimentology, v. 70, p. 1472–1495, doi:10.1111/sed.13093.

Wilckens, H. et al., 2023b, Morphological properties of moat-drift systems around the world:, doi:10.1594/PANGAEA.955053.

Wilckens, H., Eggenhuisen, J.T., Adema, P.H., Hernández-Molina, F.J., Jacinto, R.S., and Miramontes, E., 2023c, Secondary flow in contour currents controls the formation of moat-drift contourite systems: Communications Earth & Environment, v. 4, p. 316, doi:10.1038/s43247-023-00978-0.

Wu, S., Yang, Z., Wang, D., Lü, F., Lüdmann, T., Fulthorpe, C., and Wang, B., 2014, Architecture, development and geological control of the Xisha carbonate platforms, northwestern South China Sea: Marine Geology, v. 350, p. 71–83, doi:10.1016/j.margeo.2013.12.016.

Yin, S., Hernández-Molina, F.J., Lin, L., Chen, J., Ding, W., and Li, J., 2021, Isolation of the South China Sea from the North Pacific Subtropical Gyre since the latest Miocene due to formation of the Luzon Strait: Scientific Reports, v. 11, p. 1562, doi:10.1038/s41598-020-79941-4.

Yu, K., Alves, T.M., Li, W., Li, S., Li, J., Zhao, F., Wu, S., and Zhan, W., 2022, The Role of Bottom Currents on the Morphological Development Around a Drowned Carbonate Platform, NW South China Sea: Journal of Ocean University of China, v. 21, p. 801–812, doi:10.1007/s11802-022-5020-4.

FIGURE CAPTIONS

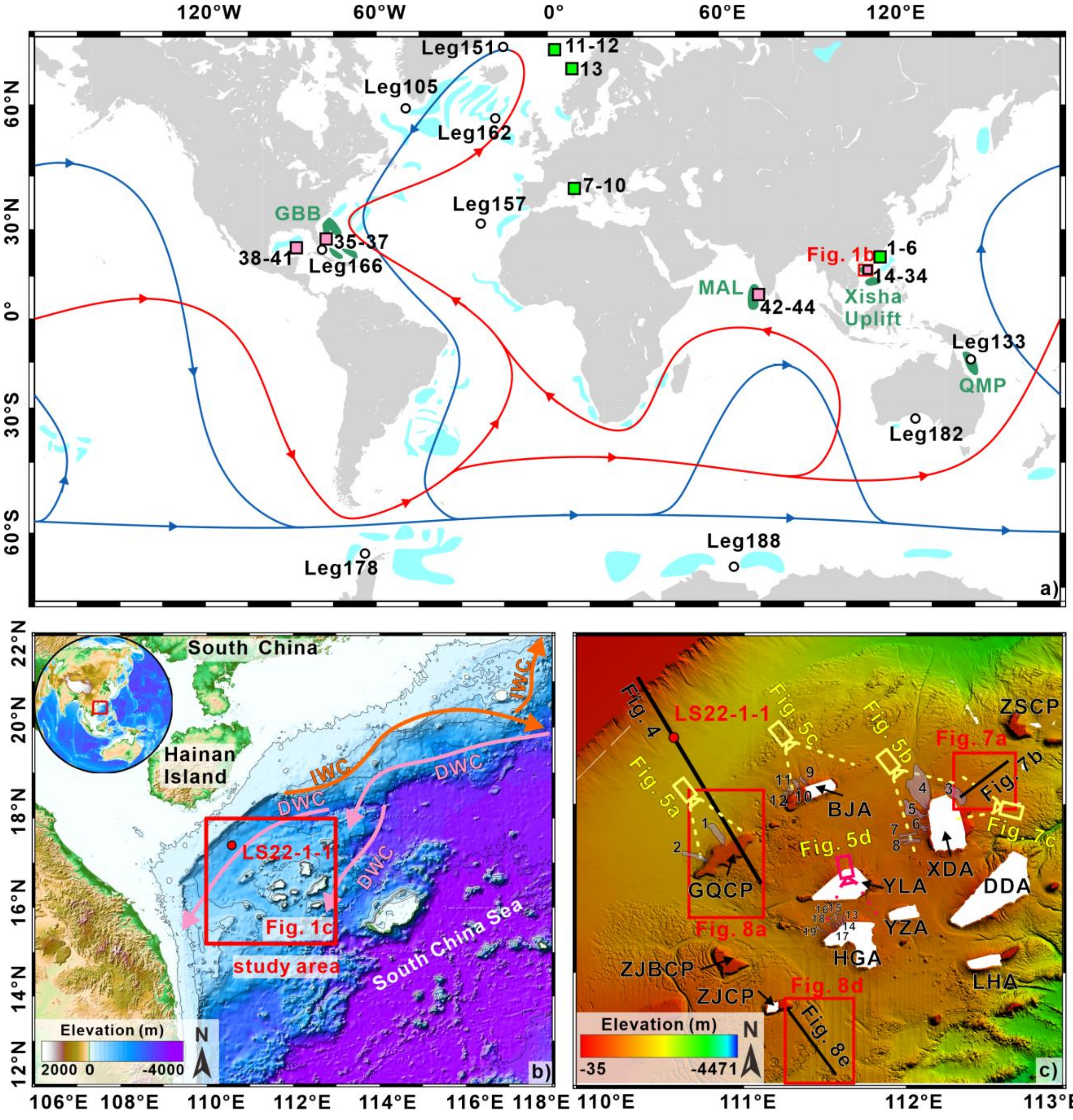

Figure 1 (a) Global distribution of contourite drifts in the world's oceans. Contourite drifts were classified into two types based on their location: (1) contourite drifts on siliciclastic continental slopes (in light blue) and (2) contourite drifts accumulated around carbonate platforms and atolls (in dark green). Figure is modified from Rebesco et al. (2014). Key areas mentioned in this work include the GBB (Great Bahama Bank), the MAL (Maldives) and the QMP (Queensland and the Marion Plateaus). Red lines and arrows show the direction of surface water flow, while the dark blue lines and arrows indicate deep-water flow direction. The locations of failed plastered drifts included in Fig.

9b are respectively marked in light green squares near siliciclastic continental slopes and as pink squares near carbonate platforms and atolls. ODP sites are marked by white circles and labelled in the figure. (b) Bathymetric map of the northern South China Sea and its oceanographic context. Intermediate (IWC) and Deep Water Currents (DWC) are highlighted on the map. The red box shows the location of the study area. (c) Zoomed-in bathymetric map of the study area, modified from Bai et al. (2022), showing the location of the seismic profiles used in this study. The red rectangles represent the extent of high-resolution multibeam bathymetric maps of the carbonate platforms and atolls depicted in Figures 7a, 8a, and 8d. The “camera” symbols near the yellow dotted lines point out to the 3D visualization of carbonate platforms/atolls in Figures 5a-d and 7c. Landslide scarps identified in this study are shown as grey polygons. Red dot marks the location of well LS22-1-1. GQCP: Ganquan carbonate platform; ZJBCP: Zhongjianbei carbonate platform; ZJCP: Zhongjian carbonate platform; ZSCP: Zhaoshu carbonate platform; BJA: Beijiao Atoll; HGA: Huangguang Atoll; LHA: Langhua Atoll; YZA: Yuzhuo Atoll; DDA: Dongdao Atoll; YLA: Yongle Atoll; XDA: Xuande Atoll.

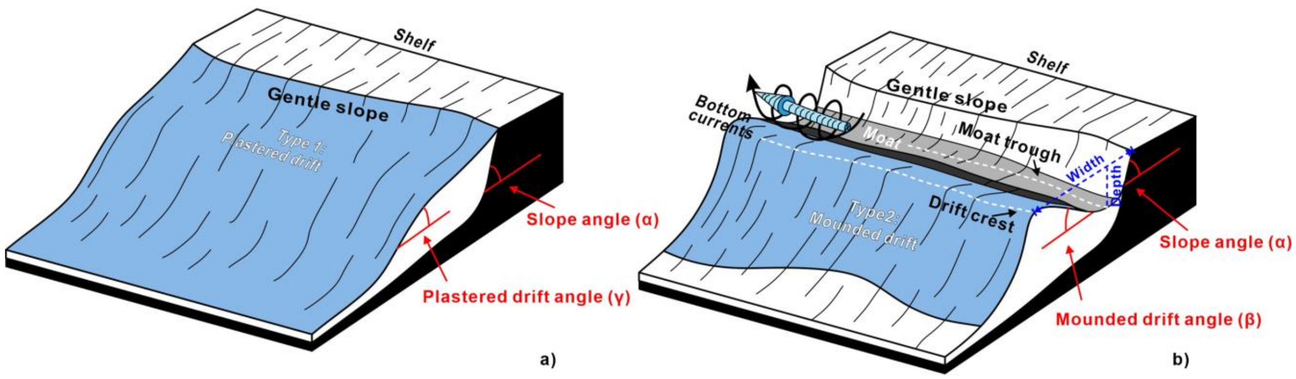

Figure 2 3D diagrams summarizing how the calculations for (a) angles of the plastered drifts and the relevant slope angles, and (b) angles of the mounded drifts and the relevant slope angles, were developed in this work. Two distinct styles of contourite drifts, distinguished by their geometry (in blue), are shown. Type 1 represents plastered drifts, while Type 2 denotes mounded drifts. Figure is modified from Hernández-Molina et al. (2008).

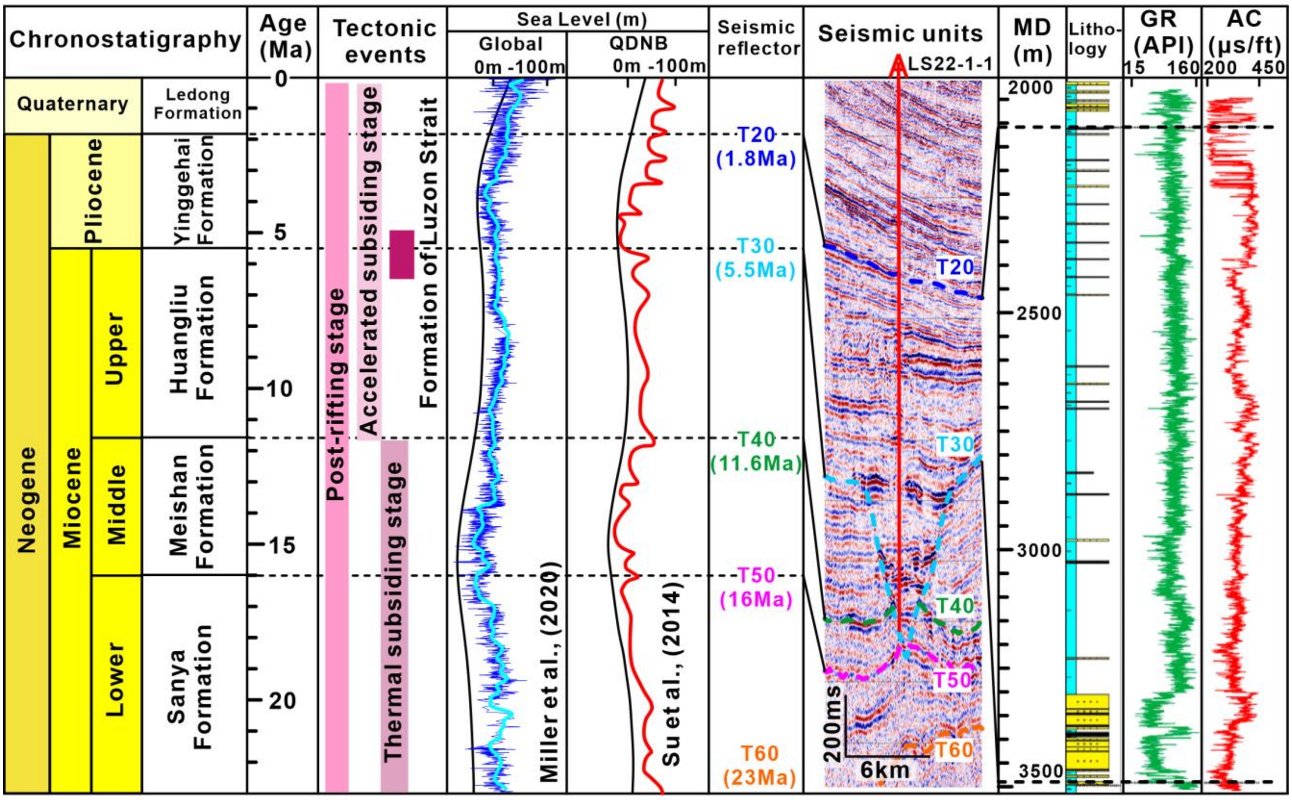

Figure 3 Stratigraphic column of the Qiongdongnan Basin documenting the lithology, sequence stratigraphic framework, and well log data for well LS22-1-1 as taken from Cheng et al. (2021). Global sea level curve is derived from Miller et al. (2020). Sea level curve for the Qiongdongnan Basin is based on Su et al. (2014). Tectonic events depicted in this column are modified from Wang et al. (2022). MD: Measured Depth; GR: Gamma Ray; AC: Acoustic Slowness (μs/ft).

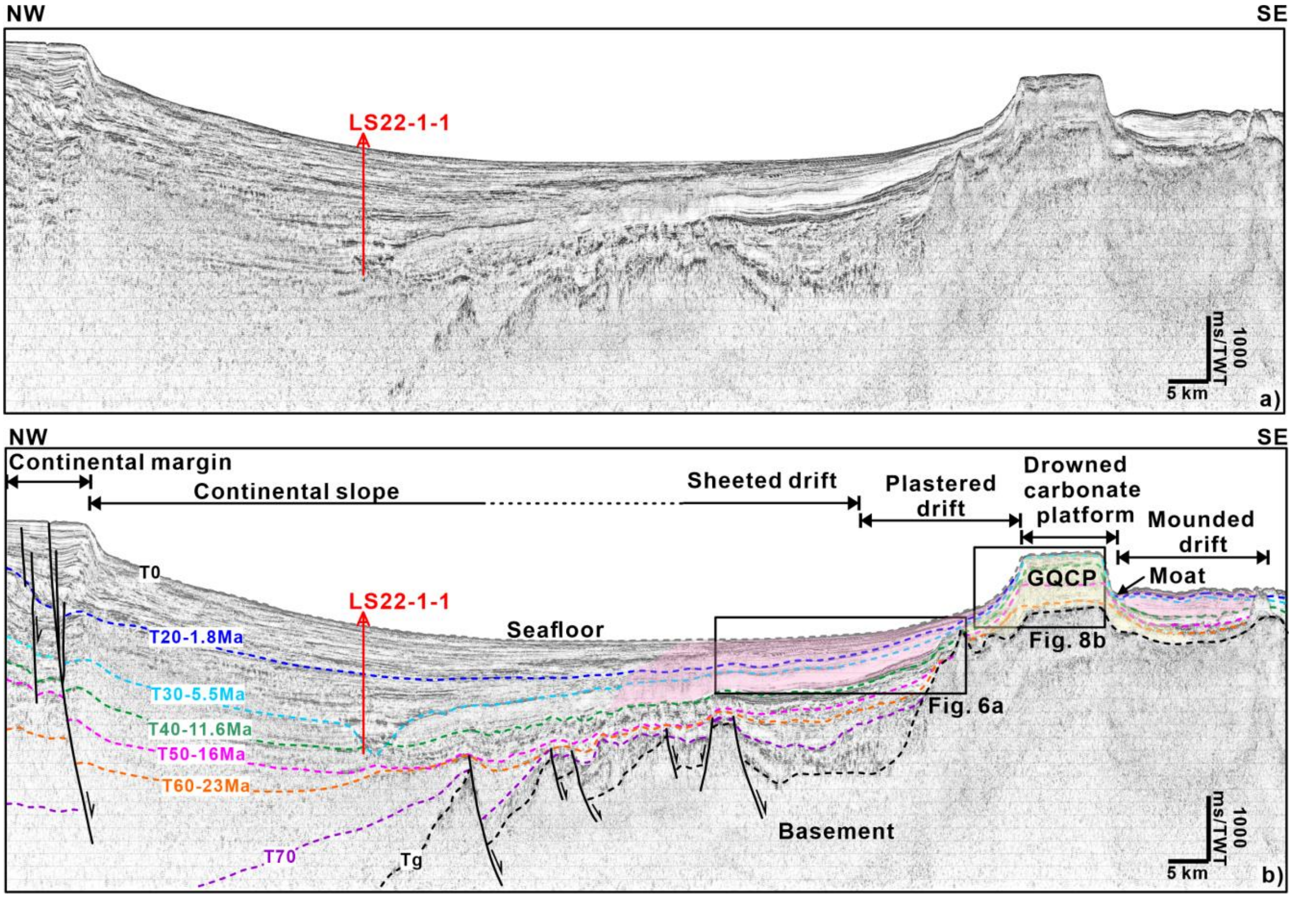

Figure 4 (a) Uninterpreted and (b) interpreted NW-SE 2D seismic profile across the continental slope to the northwest and the Ganquan carbonate platform (GQCP) on the Xisha Uplift. The location of this seismic profile is shown in Figure 1c. Eight seismic reflectors (T0 to Tg) are labelled in the interpreted seismic profile. Contourite drifts reveal sub-parallel and continuous seismic facies and are mainly located around the Ganquan carbonate platform (GQCP). Plastered and mounded drifts are distributed on the carbonate platform's western and eastern flanks, respectively. TWT: two-way travel time; GQCP: Ganquan carbonate platform.

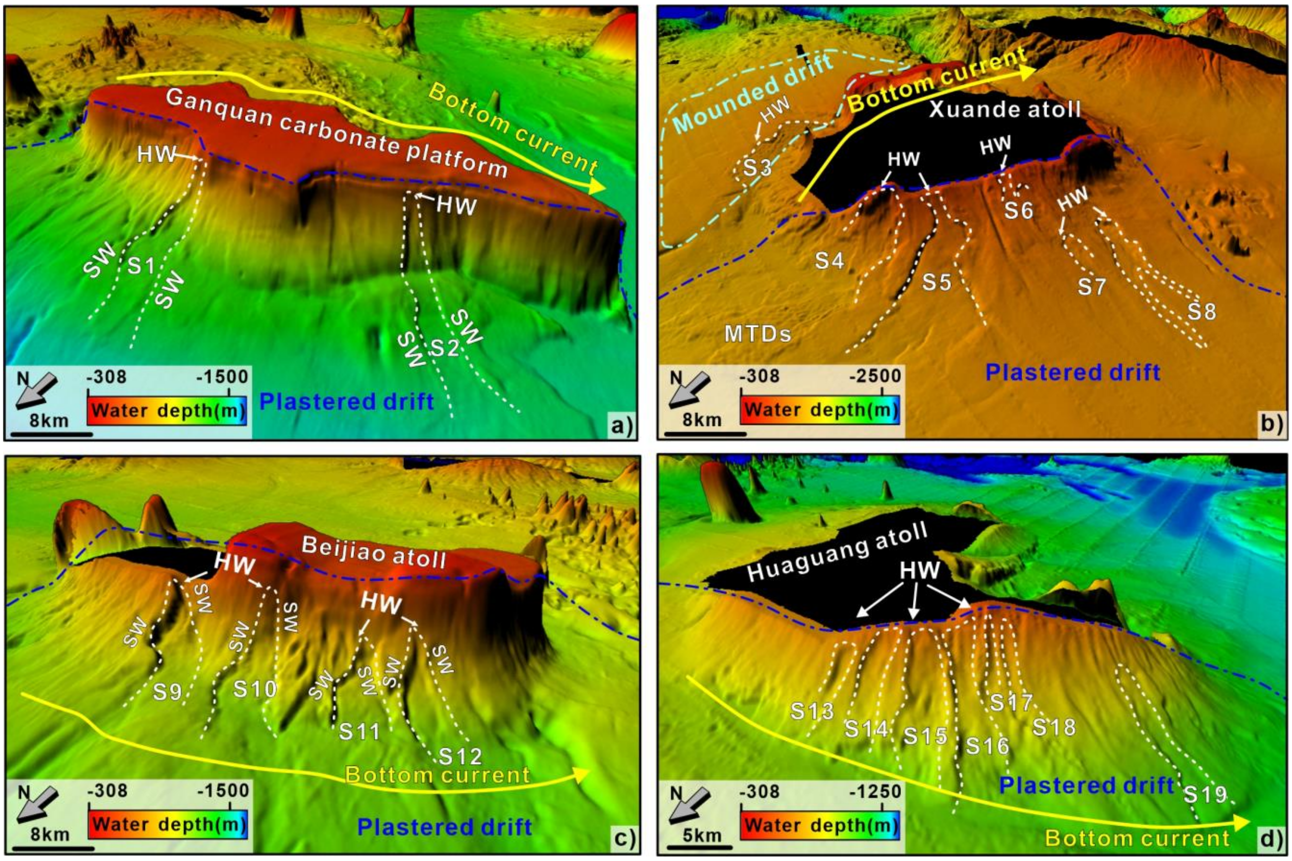

Figure 5 Three-dimensional views of the (a) Ganquan carbonate platform (GQCP), (b) Xuande Atoll (XDA), (c) Beijiao Atoll (BJA), and (d) Huaguang Atoll (HGA). The multibeam bathymetry maps reveal the occurrence of multiple submarine landslides around these carbonate platforms and atolls (shown in Figure 1c). The geomorphological characteristics of the identified submarine landslides, such as their area and volume, are listed in Table 1. HW: headwall; SW: sidewall; S: slide. The white dotted line shows the boundary between headscarp and sidewall. Dark blue dash-dotted line indicates the depositional boundary of plastered drifts. Yellow solid line illustrates the direction of bottom current.

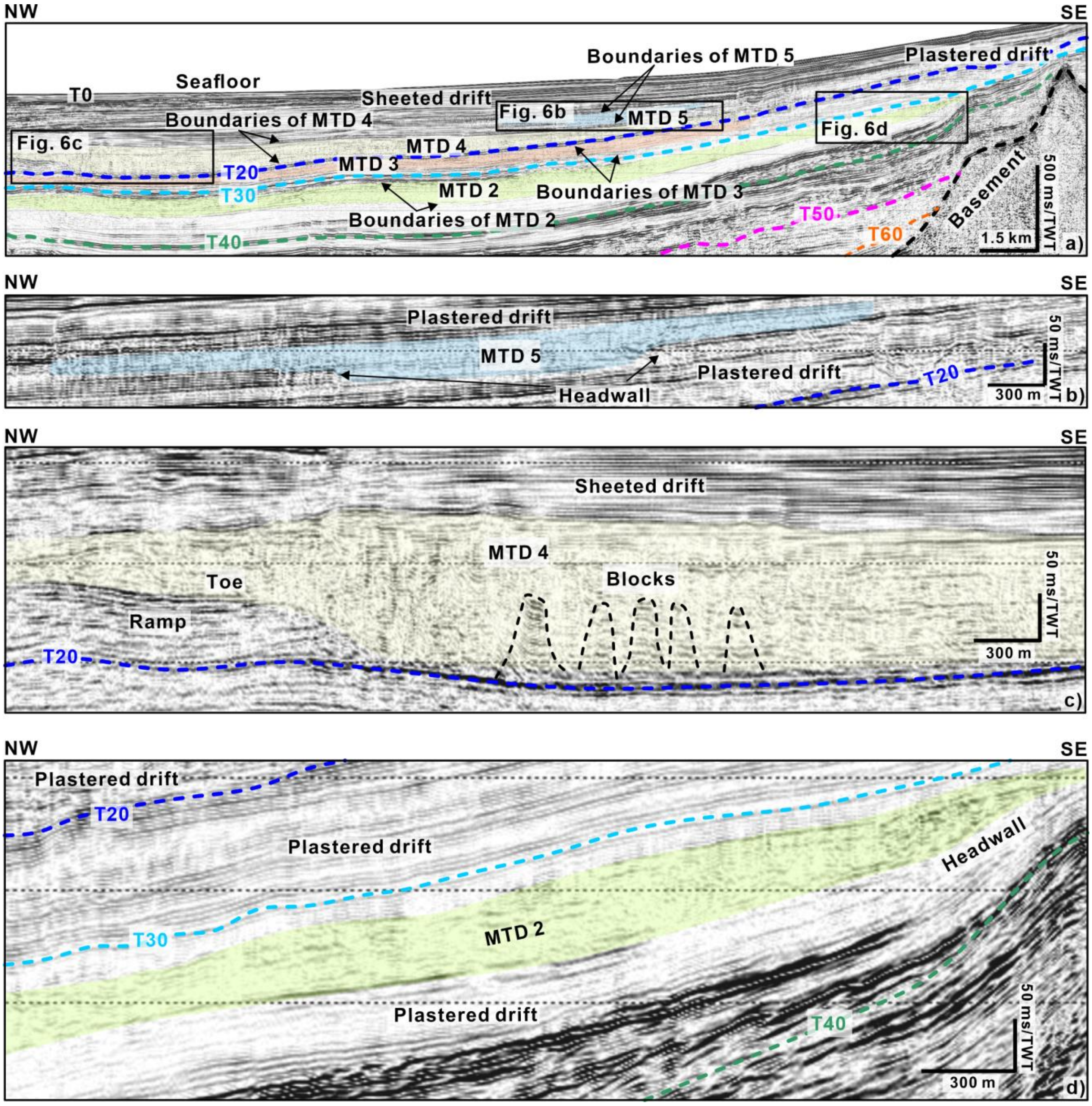

Figure 6 (a) Seismic profile crossing the northwest flank of the Ganquan carbonate platform (GQCP), revealing a widespread deposition of plastered drifts and mass-transport deposits (MTDs) in this area. Location of the seismic profile is shown in Fig. 4b. Figs. 6b, 6c and 6d are zoomed-in seismic profiles that highlight the internal seismic architecture of MTDs. MTDs: mass transport deposits. TWT: two-way travel time.

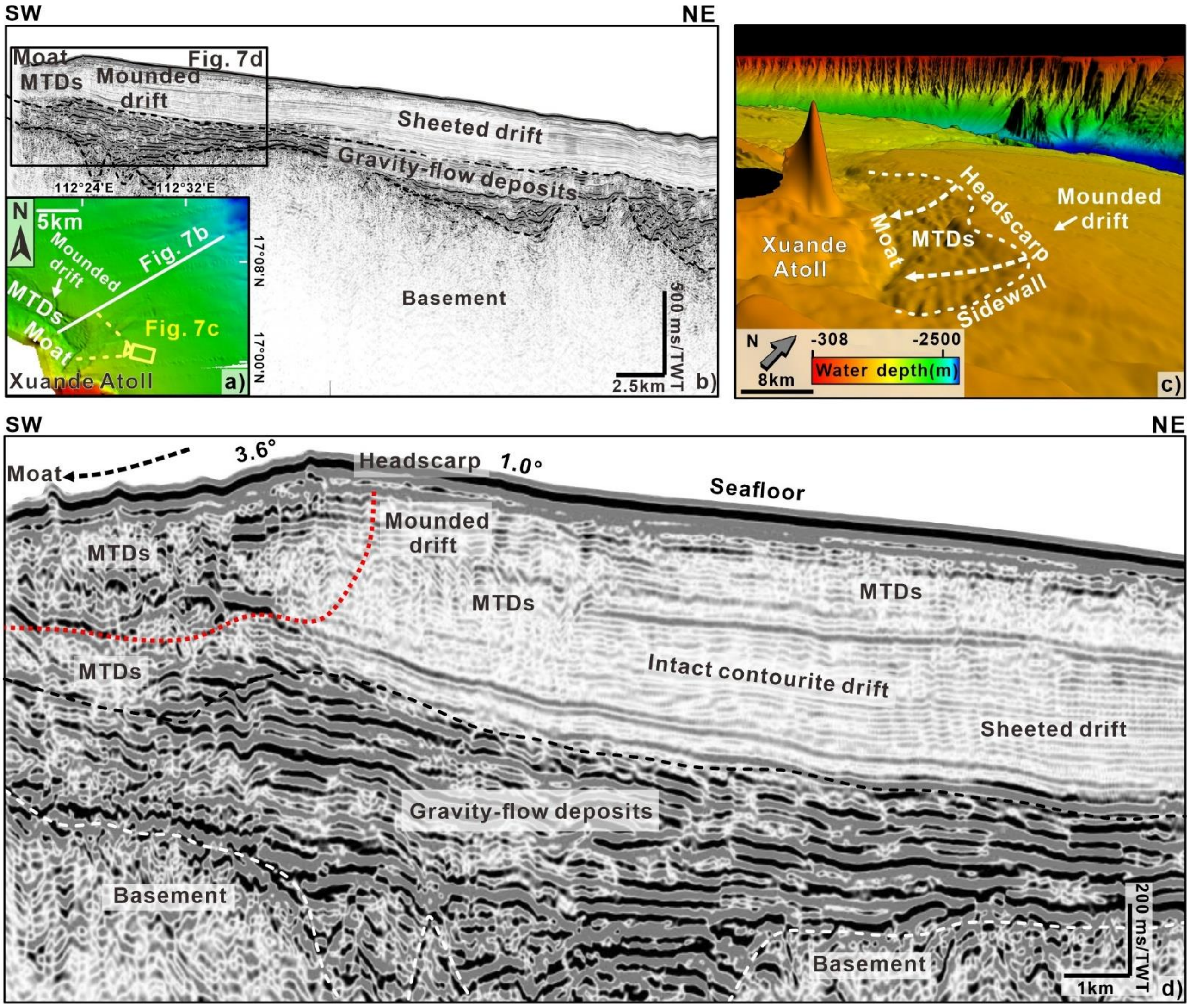

Figure 7 (a) Multibeam bathymetric map revealing the main morphological features surrounding a carbonate platform or atoll. (b) 2D seismic profile revealing the seismic facies of contourite drifts on the northeast flank of the Xuande Atoll (XDA). (c) 3D view of slope failure on mounded drifts. (d) Zoomed-in seismic profile highlighting the internal structure of MTDs, mounded drifts and sheeted drifts.

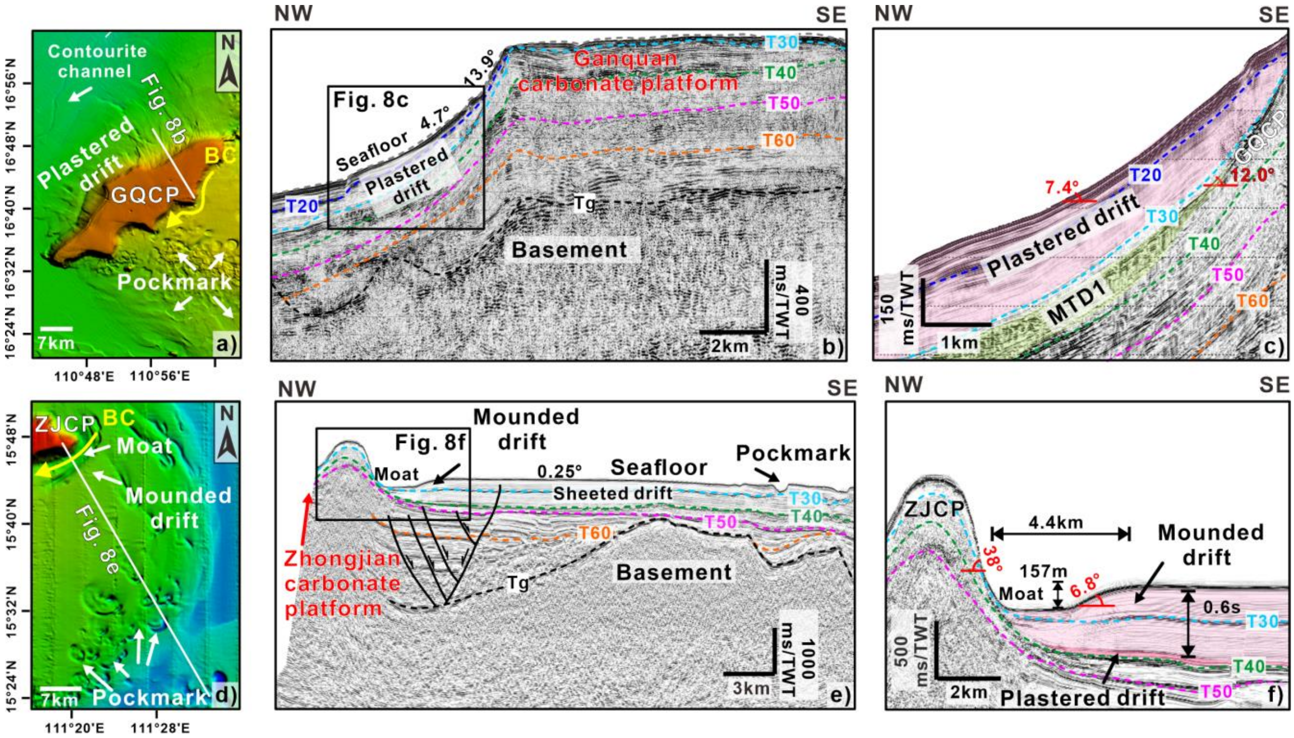

Figure 8 (a) and (d) Multibeam bathymetric maps of the Ganquan (GQCP) and Zhongjian (ZJCP) carbonate platforms, showing the location of (b) and (e) as well as the directions of bottom currents. (b) and (e) 2D seismic profiles imaging plastered and mounded drifts around the two carbonate platforms. (c) and (f) Zoomed-in seismic profiles illustrating the internal architecture of these drifts. Plastered and mounded drifts are highlighted in pink color. BC: bottom current; GQCP: Ganquan carbonate platform; ZJCP: Zhongjian carbonate platform; TWT: two-way travel time.

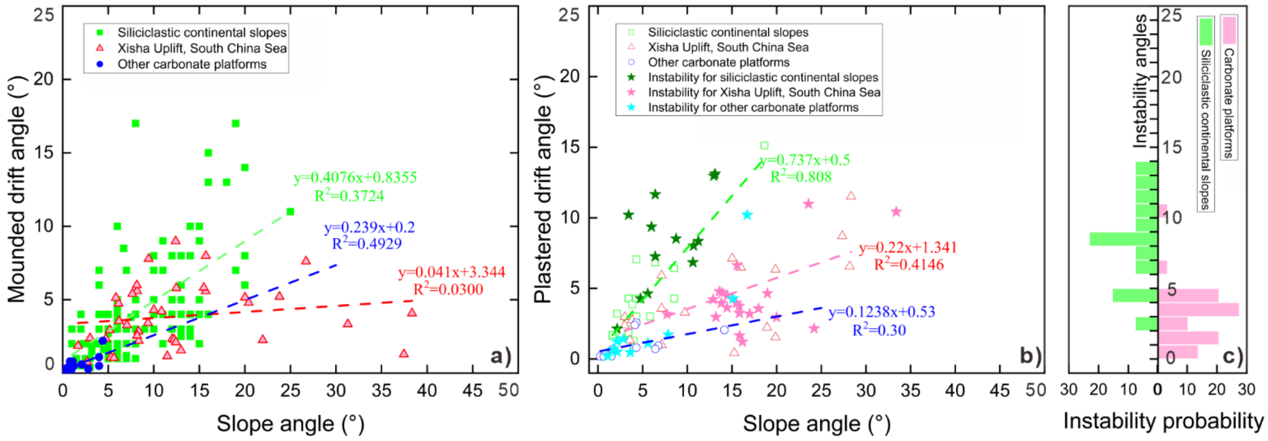

Figure 9 (a) Scatter diagrams and corresponding linear regressions highlighting the relationship between slope angle and mounded drift angle on siliciclastic continental slopes across the world and around carbonate platforms/atolls. Green square dots represent the angles of siliciclastic continental slopes, the pink triangle dots represent the angles around the Xisha carbonate platforms/atolls (study area), and the dark blue dots indicate the angles from other carbonate platforms, e.g. Bahamas, Maldives and northeast Australia (see Supplementary Table 02). (b) Scatter diagrams showing the relationship between slope angle and plastered drift angle (see Supplementary Table 01). The stars in dark green, pink and light blue respectively point out to the instability of plastered drifts on siliciclastic continental slopes, on the Xisha Uplift, and near other carbonate platforms/atolls (see Fig. 1a for location and Supplementary Table 04). (c) Bar chart showing the distribution of dip angle of failed plastered drifts on siliciclastic continental slopes across the world and around carbonate platforms/atolls. The methods for measuring these angles are illustrated in Figs 2a and 2b. The green and pink bars show the probability of finding unstable plastered drifts as a function of slope angle.

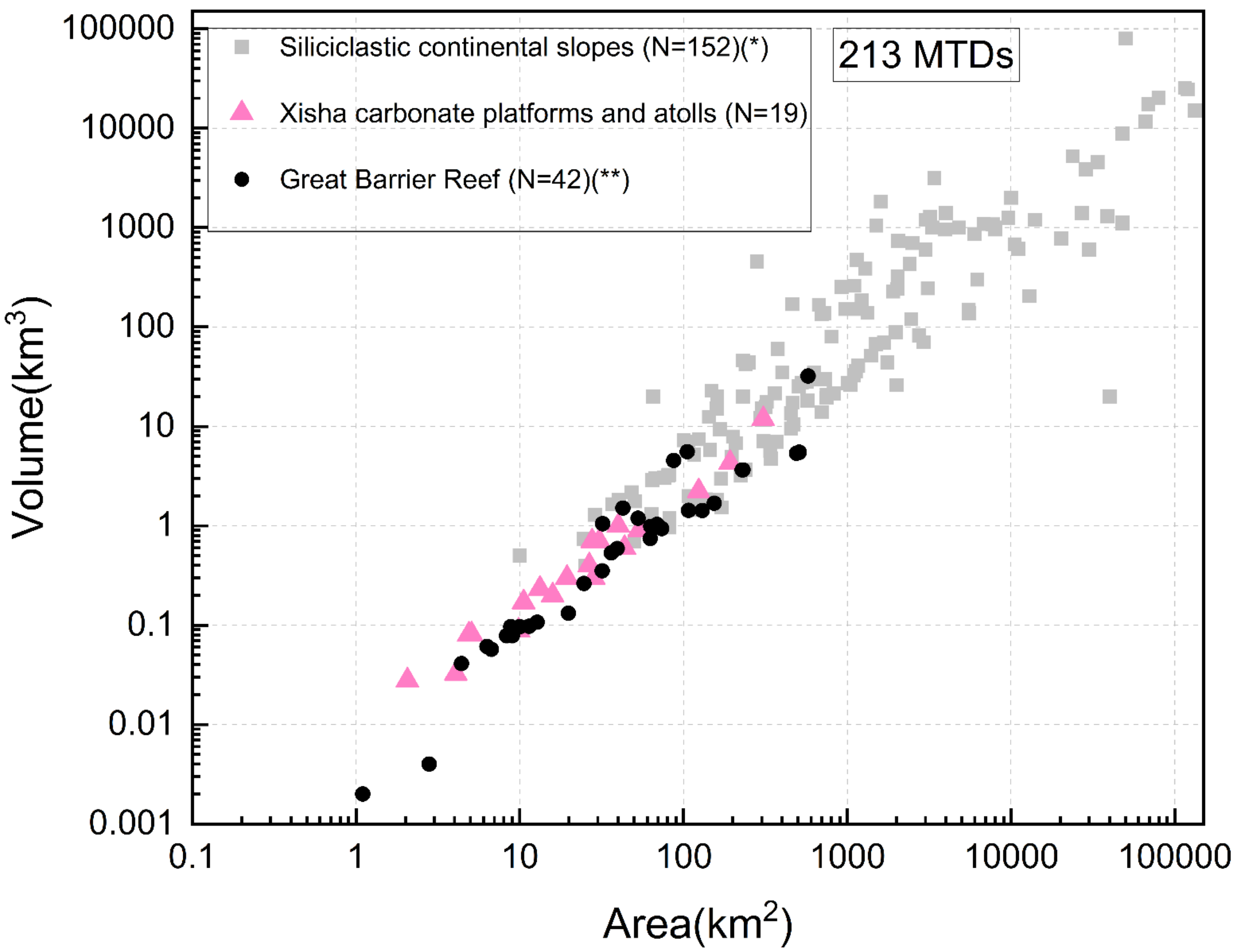

Figure 10 Scatter diagrams highlighting the relationship between the volume and area distribution of 213 MTDs on siliciclastic continental slopes and surrounding carbonate platforms/atolls. The pink triangles represent MTDs on the Xisha Uplift (see Table 1 for area and volume of slides in this study). The black dots represent MTDs around the Great Barrier Reef of northeast of Australia. The grey squares represent the MTDs on siliciclastic continental slopes across the world. (*) from Moscardelli and Wood. (2015) and (**) from Puga-Bernabéu et al. (2022).

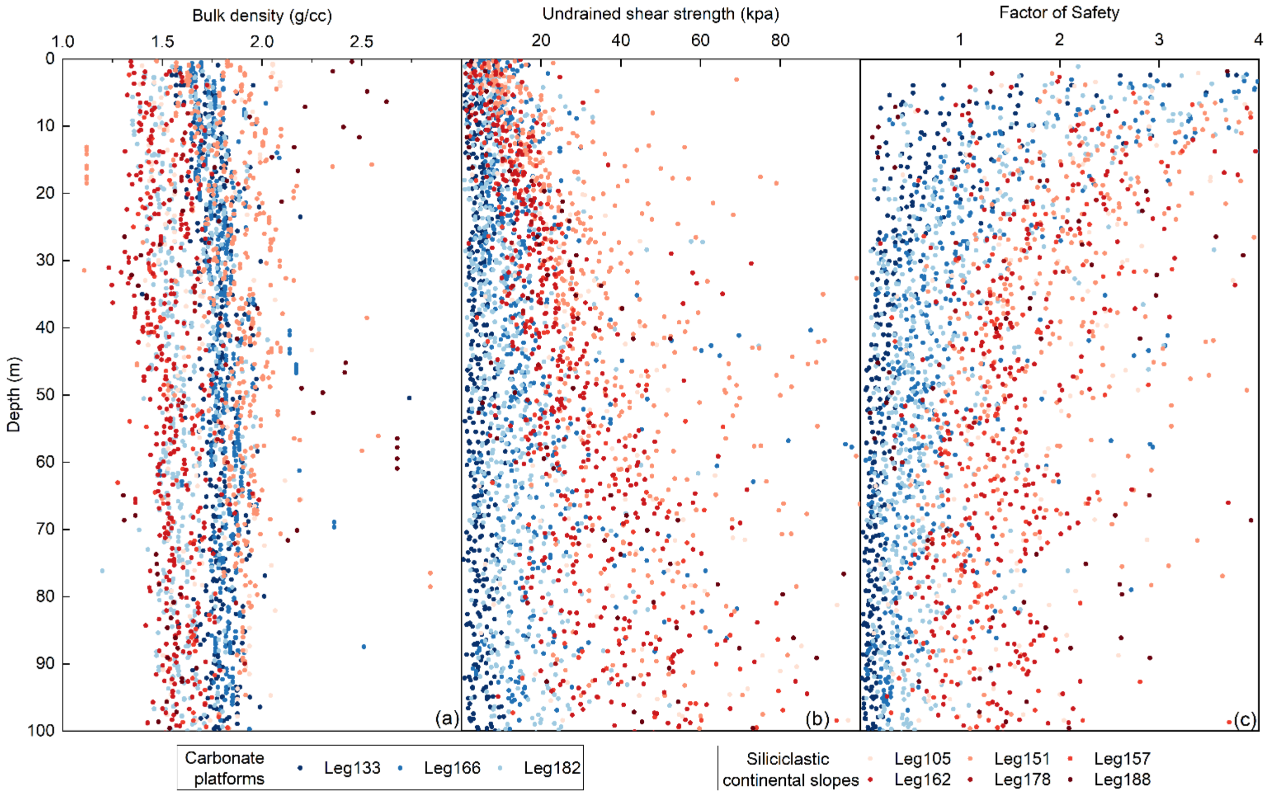

Figure 11 Scatter diagrams for: (a) Bulk density, (b) Undrained shear strength and (c) Factors of Safety (FOS) with depth, for different deep-sea depositional environments where contourite drifts develop. These environments include open siliciclastic continental slopes (indicated by warm-colored dots; ODP Legs 105, 151, 157, 162, 178 and 188), and carbonate platforms/atolls (indicated by cold-colored dots; ODP Legs 133, 166 and 182). Data are extracted from the Ocean Drilling Program data archives (Please see Figure 1a for locations and Supplementary Table 03).

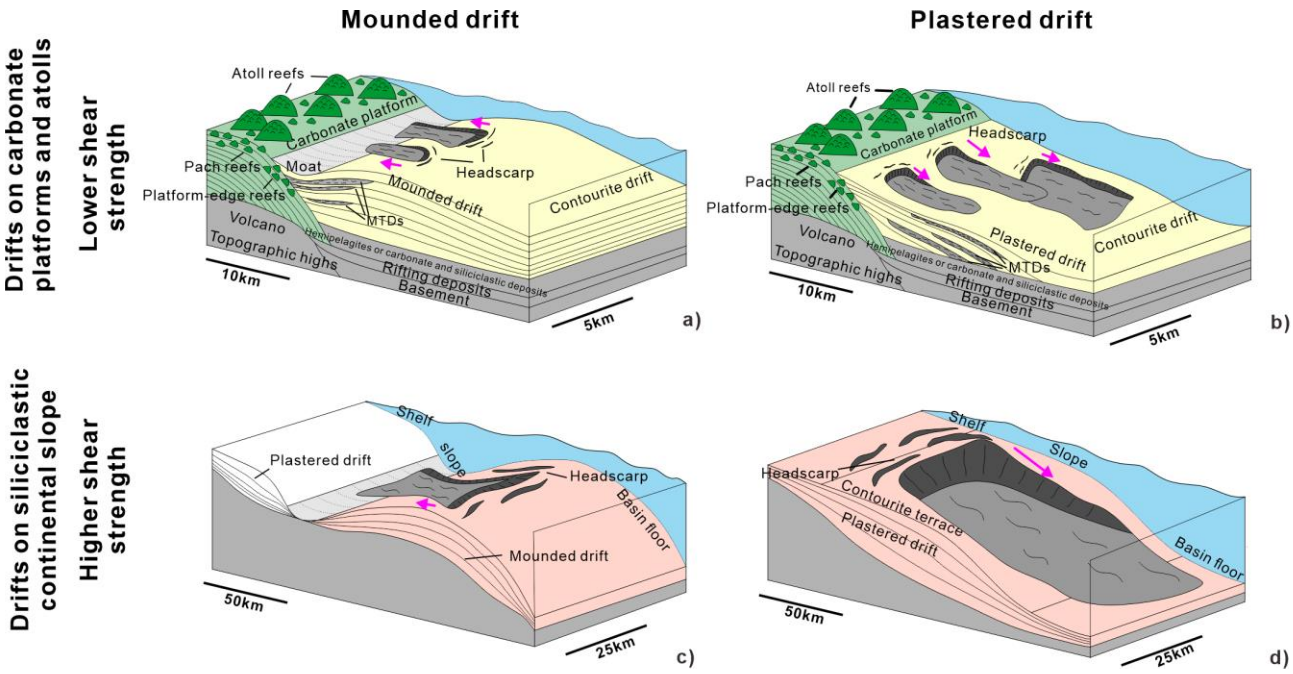

Figure 12 3D models depicting the instability of contourite drifts in two different deep-water environments. (a) and (b) represent the instability of mounded and plastered drifts surrounding carbonate platforms/atolls. (c) and (d) show the instability of mounded and plastered drifts with higher drift angles along siliciclastic continental slopes.

Number of landslides	Latitude and longitude	Frontal confinement	Depth below seafloor (m)	Scar perimeter length, Ls (km)	Headscarp height, Hs (m)	Scar width, Ws (km)	Slope gradient, S (°)	Slope gradient of the headscarp, Ss (°)	Volume (km^3)	Area (km^2)
1*	110.908, 16.757	frontally emergent	1329	8.06	55.069	2.92	9.05	12.56	0.700	30.600
2*	110.807, 16.657	frontally emergent	1293	7.375	39.072	2.124	7.97	11.29	0.300	28.400
3	112.365, 17.080	frontally emergent	953	21.609	46.016	15.129	1.72	2.8	2.232	124.000
4*	112.165, 16.993	frontally emergent	1055	24.6	89.215	12.807	3.13	15.51	11.800	306.600
5*	112.149, 16.927	frontally emergent	843	30.284	56.979	5.284	3.12	4.36	4.300	192.600
6*	112.159, 16.856	frontally emergent	637	9.839	49.547	4.772	3.58	10.28	0.400	26.600
7*	112.091, 16.822	frontally emergent	840	10.164	23.587	2.577	0.98	5.37	0.600	43.600
8*	112.107, 16.774	frontally emergent	865	18.347	64.523	2.602	0.69	8.42	0.200	15.900
9*	111.415, 17.123	frontally emergent	903	8.776	83.658	2.006	5.22	16.13	0.700	27.600
10*	111.365, 17.103	frontally emergent	967	12.467	63.095	3.433	7.76	12.87	0.300	19.400
11*	111.322, 17.074	frontally emergent	963	8.935	50.587	1.564	10.69	13.31	0.900	53.700
12*	111.307, 17.057	frontally emergent	993	7.477	51.657	1.168	10.21	10.86	1.000	40.000
13	111.655, 16.303	frontally emergent	698	4.866	27.475	0.856	2.75	9.11	0.028	2.065
14	111.643, 16.290	frontally emergent	705	8.351	30.931	1.525	3.31	8.69	0.080	4.879
15	111.626, 16.276	frontally emergent	730	11.115	26.236	2.057	4.69	5.66	0.170	10.540
16	111.609, 16.265	frontally emergent	568	10.624	30.288	1.592	5.28	10.88	0.233	13.307
17	111.601, 16.252	frontally emergent	570	7.972	20.709	0.618	4.08	6.41	0.032	4.069
18	111.595, 16.251	frontally emergent	582	7.602	17.738	0.736	4.39	6.23	0.081	5.068
19	111.521, 16.238	frontally emergent	788	14.958	17.638	1.178	3.04	4.41	0.088	9.839

Table 1 The geographic characters of submarine landslides on the Xisha Uplift. Asterisk (*) highlights the submarine landslides from which volume and area measurements are derived from Bai et al. (2022).